A PLANAR CAVITY BACKED SLOT ANTENNA ARRAY FOR ULTRA-WIDEBAND AUTOMOTIVE MONOPULSE RADARS

by

VINAY MAGADI VIKRAM

Presented to the Faculty of the Graduate School of
The University of Texas at Arlington in Partial Fulfillment
of the Requirements
for the Degree of

MASTER OF SCIENCE IN ELECTRICAL ENGINEERING

THE UNIVERSITY OF TEXAS AT ARLINGTON

May 2010

Copyright © by VINAY MAGADI VIKRAM 2010

All Rights Reserved

To my mother, father and brother

ACKNOWLEDGEMENTS

I would like to express my deep and sincere gratitude to my supervisor Dr. Mingyu Lu. His stimulating suggestions and encouragement helped me throughout my research. I also gained a lot of knowledge from his thorough understanding of the research area and his tutoring methods.

I would like to thank Sha Shaoshu and Vitthal Kodgirwar for their help during simulation and practical antenna testing in the anechoic chamber. I would also like to thank Dr. Huiqing Zhai for helping me with the Ansoft HFSS simulations.

I am indebted to my family, my Mother Annapurna, my Father Vikram and my Brother Vivek for their unyeilding love and support throughout my entire life. Finally I would like to thank all my friends who have been like a second family during my masters' study.

April 19, 2010

ABSTRACT

A PLANAR CAVITY BACKED SLOT ANTENNA ARRAY FOR ULTRA-WIDEBAND AUTOMOTIVE MONOPULSE RADARS

VINAY MAGADI VIKRAM, M.S.

The University of Texas at Arlington, 2010

Supervising Professor: MINGYU LU

In this thesis, a wideband cavity backed slot antenna is designed for automotive-borne monopulse radar applications. A rectangular slot is used to realize broad bandwidth; the slot is backed by a cavity and vertical walls of the cavity are implemented by discrete vias; and the slot is fed by an inverted microstrip line. The antenna in this letter is compact, robust, fully planar, and easy to integrate. A two-element array is fabricated and tested. Measured input impedance is matched to 50 Ω within band [2.61 GHz, 3.44 GHz] (27.5% bandwidth); and monopulse beam-scanning is successfully demonstrated.

TABLE OF CONTENTS

ACKNOWLEDGEMENTS iv

ABSTRACT v

LIST OF FIGURES viii

LIST OF TABLES x

Chapter Page

1. INTRODUCTION 1

1.1 Introduction 1

1.2 Automotive-borne Radars 1

1.2.1 Short Range Radars (SRR) 2

1.3 Existing Antennas Used In Short Range Radars (SRR) 4

1.3.1 Planar Radiators 5

1.4 The Proposed Cavity Backed Slot Antenna 6

1.4.1 Use of Discrete Cavity Wall Backing 7

1.5 Organization Of This Thesis 7

2. CAVITY BACKED SLOT ANTENNA DESIGN 9

2.1 Introduction 9

2.2 Initial Design 10

2.2.1 Cavity Backed Loop Slot Antenna 10

2.2.2 Two Element Cavity Backed Loop Slot Antenna Array 10

2.3 Improved Design 12

2.3.1 Cavity Backed Rectangular Slot Antenna 12

2.3.2 Cavity Backed Rectangular Slot Antenna Array 14

3. SIMULATION, CALIBRATION AND MEASUREMENT METHODS . . 17
3.1 Introduction . . . 17
3.2 Simulation using Ansoft HFSS . . . 17
3.2.1 3-D Cavity Backed Slot Antenna Model Development . . . 17
3.3 Fabrication Procedure . . . 19
3.4 Pattern Measurement Methods . . . 22
3.5 Three Antenna Method . . . 25
3.5.1 Monopulse Beam Scanning . . . 25
3.6 TRL Calibration . . . 26
3.6.1 Line Length Design . . . 26
3.6.2 De-embedding of DUT . . . 27
4. RESULTS AND DISCUSSION . . . 30
4.1 Introduction . . . 30
4.2 CBS Element Results . . . 30
4.2.1 Single Element Input Impedance Result . . . 30
4.2.2 Single Element Pattern Measurement Results . . . 30
4.3 Two Element Array Results . . . 32
4.3.1 Two Element Array Input Impedance Results . . . 32
4.3.2 Two Element Array Forward Pattern Results . . . 33
4.3.3 Two Element Array Forward Null Pattern Results . . . 34
4.3.4 Two Element Array Beamscan Pattern Results . . . 36
4.3.5 Two Element Array Beamscan Null Pattern Results . . . 42
4.4 Results Overview . . . 43
5. CONCLUSIONS . . . 45
REFERENCES . . . 47
BIOGRAPHICAL STATEMENT . . . 52

LIST OF FIGURES

Figure		Page
1.1	Complete environment sensing for automobiles [15]	3
2.1	Cavity backed loop slot antenna (a) Top view, (b) Side view	11
2.2	Loop CBS antenna array (a) Full view, (b) Top view, (c) Cut view	12
2.3	Fabricated prototype of cavity backed loop slot antenna array	13
2.4	Inverted CBS antenna (a) Disassembled view, (b) Top view	14
2.5	Fabricated inverted CBS antenna element front view	14
2.6	Fabricated inverted CBS antenna element bottom view	15
2.7	Prototype of inverted CBS antenna array front view	16
2.8	Prototype of inverted CBS antenna array bottom view	16
3.1	Design Flow in Ansoft HFSS [35]	18
3.2	3-D Model of cavity backed slot antenna element	19
3.3	3-D Model of two element cavity backed slot antenna array	20
3.4	Antenna pattern measurement co-ordinate system [7]	23
3.5	Instrumentation for an antenna range measurement system [7]	24
3.6	Feed structure of the two-element array	26
4.1	Input impedance of inverted cavity backed slot antenna element	31
4.2	Broadside radiation pattern at 2.8 GHz	31
4.3	Broadside radiation pattern at 2.9 GHz	32
4.4	Broadside radiation pattern at 3.0 GHz	33
4.5	Broadside radiation pattern at 3.1 GHz	34
4.6	Broadside radiation pattern at 3.2 GHz	35

4.7 Input impedance of inverted cavity backed slot antenna element . . . 35
4.8 Input impedance of inverted cavity backed slot antenna element . . . 36
4.9 Broadside forward radiation pattern at 2.8 GHz 36
4.10 Broadside forward radiation pattern at 2.9 GHz 37
4.11 Broadside forward radiation pattern at 3.0 GHz 37
4.12 Broadside forward radiation pattern at 3.1 GHz 38
4.13 Broadside forward radiation pattern at 3.2 GHz 38
4.14 Broadside forward radiation pattern at 3.3 GHz 39
4.15 Broadside forward null radiation pattern at 2.8 GHz 39
4.16 Broadside forward null radiation pattern at 3.0 GHz 40
4.17 Broadside forward null radiation pattern at 3.2 GHz 40
4.18 Broadside beamscan radiation pattern at 3.0 GHz 41
4.19 Broadside beamscan radiation pattern at 3.1 GHz 41
4.20 Broadside beamscan radiation pattern at 3.2 GHz 42
4.21 Broadside beamscan null radiation pattern at 3.0 GHz 43
4.22 Broadside beamscan null radiation pattern at 3.2 GHz 44

LIST OF TABLES

Table Page

1.1 Summary of typical short-range sensor system requirements [15] . . . 4

3.1 Model Development Summary 18

CHAPTER 1

INTRODUCTION

1.1 Introduction

In the second section of this chapter an overview of automobile-borne radar systems is given highlighting the different types of automotive radar systems in existance and their spectrum of operation. Special attention is given to the description of short range radars as the planar antenna discussed in this thesis report finds its application in such radars. In the third section a brief description of existing antennas is given with a focus on planar slot and patch radiators. In the fourth section a brief note of the proposed cavity backed slot (CBS) antenna design is mentioned. The chapter concluded with an overview of the thesis report.

1.2 Automotive-borne Radars

The subject of automotive radar is not new, and developments have been occurring on a regular basis, as reported in the technical literature for many years [28]. One of the main barriers to widespread introduction to date has been the ability to fulfil the extremely demanding technical requirements at a cost level that the average consumer will find palatable. Due to the strong support that the introduction of such sensors has from the automotive industry, significant advancements have been made to introduce automotive radars for wide scale commercial use [1].

Recently the approval granted by the Federal Communications Commission (FCC), the subject of much interest and controversy [5, 2, 27, 30, 34] for the use of ultra-wideband signals for vehicular radar applications has provided a gateway for the

introduction of these sensors in the commercial arena as early as 2004. The approval allocates over 7 GHz of usable unlicensed spectrum over two separate frequency spectrums [11]. The first allocation of an unlicensed 7 GHz spectrum i.e. 3.1 GHz to 10.6 GHz is for communication and imaging systems based on ultra wideband (UWB) devices. The second allocation of unlicensed spectrum i.e. 22 GHz to 29 GHz is intended exclusively for vehicular radar systems. These systems are intended to detect the location and movement of objects near a vehicle by developing a continuously updated 360^0 -radar map of the vehicles surroundings. Due to the requirement of having 360^0 coverage around the car a single sensor is clearly not a suitable solution, and a system comprised of multiple networked sensors that are distributed at appropriate locations is required.

Due to the multiplicity of various driving and traffic scenarios, a variety of active safety systems that provide automatic intervention and passive safety systems that provide driver information, are required to give a vehicle the capability to not only perceive and understand its environment, but to also act upon it. In terms of traffic and object awareness, the important systems are mainly video, infrared (IR) and radar based [41, 9]. A typical schematic of one of these sensor arrays is shown in Figure 1.1. A radar system is perceived as a key element in the sensor array due to its ability to offer an immunity to weather conditions that is unavailable with the other existing technological solutions.

1.2.1 Short Range Radars (SRR)

The demands of short-range radar sensors have increased because they can be applied to various applications, such as automotive radar sensors, healthcare sensors and motion detectors [19, 20, 10, 14, 4]. To be used in those applications, radar sensors must be compact and high-performing. For compact size, the operating frequency

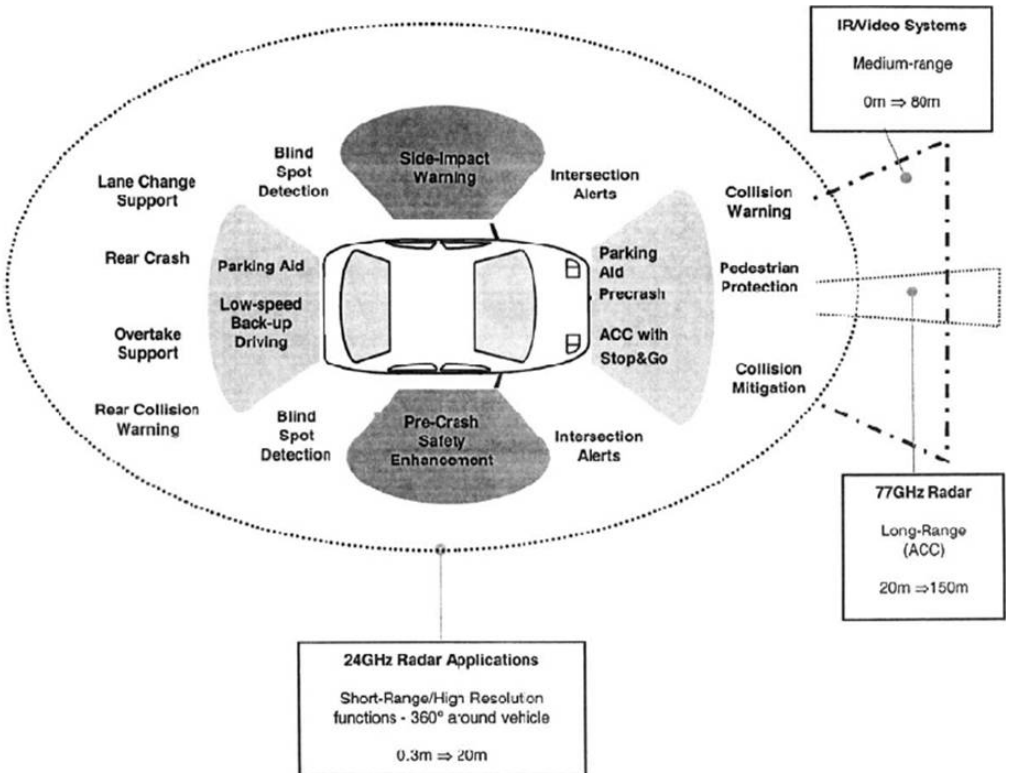

Figure 1.1. Complete environment sensing for automobiles [15].

of the radar system must be increased to a millimetre wave frequency. In short-range radar, 24 GHz in industrial, scientific, and medical bands have been widely used. The compact size of radar can be achieved with such a high frequency because the size of the passive and active components can be reduced. A single antenna radar structure is also important for reducing the size of a radar sensor because the antenna is one of the largest components of radar sensors. It is important to have high Tx-to-Rx isolation in a single antenna radar sensor.

In this report a Cavity Backed Slot Antenna is being described for use in a Short Range Radar (SRR) to increase driving safety by providing some of the following functions:

- Distance and relative velocity of the nearest obstacles.

- Parking aid.
- Pre-crash detection.
- Short range cruise control functionality.
- Blind spot detection.
- Stop and go.

A summary of key requirements in a Short Range Sensor System is given in Table 1.1.

Table 1.1. Summary of typical short-range sensor system requirements [15]

	Blind Spot	**Parking Aid**	**Stop and go**	**Simple Pre-crash**
Max. Detection Range (m)	4-8	2-5	20	7-10
Required Range Resolution (m)	0.1-0.2	0.05-0.2	0.2-0.5	0.1-0.2
Max. Relative Velocity (m/s)	15-25	3-5	8-12	40-60
Aquisition Time (ms)	200	500	300	50
Update Time (ms)	50	50	40	20
Minimum Object Size	Bicycle	3" PVC Pole	Bicycle	Metal Post

1.3 Existing Antennas Used In Short Range Radars (SRR)

A wide variety of antennas are used in SRR. The main requirements for a short range radar antenna are:

- Wide band with a bandwidth of at least 500 MHz.
- Low-cost of fabrication.
- Mechanically reliable.
- Small.

- Light weight.

In order to satisfy all these requirements a variety of designs have been proposed like luneberg lens [39], microstrip leaky wave antenna (MLWA) [25], reflectarray antenna [29], shaped dielectric lens [36], artificial lens [13], multi loop array antenna (MLAA) [31], dielectric filled antenna (DFW) [16] to name a few. Even though there are a variety of novel antenna designs for automotive-borne radar applications, printed patches are the most commonly adopted planar antenna candidates [15, 17] as their inherent characteristics like planar, conformal, ease of fabrication, mechanically reliable make them the ideal candidate to be used in car borne short range radars. However, it is challenging for patch antennas to achieve broad bandwidth; in addition, patch array suffers from mutual coupling through surface waves [32]. In this report, a novel slot antenna is designed for wideband car-borne monopulse radars.

1.3.1 Planar Radiators

The most common candidate for planar radiators are the slot antenna and patch antenna. Slot and patch radiators have several advantages in common; i.e. both are planar, conformal, and low-cost. In general the slot width of the cavity backed slot antenna is negligibly narrow in comparison with the slot length. However, the frequency bandwidth of the antenna is not enough for wideband antenna applications. In order to increase the frequency bandwidth the slot width is widened. Upon controlling this design aspect the frequency bandwidth of a cavity backed slot antenna can be significantly increased. However, in case of patch antennas to achieve broad bandwidth the thickness of the substrate is increased, leading to the patch array suffering from mutual coupling through surface waves [32]. Hence compared to patches, it is relatively easier to enlarge the slots' bandwidth by revising the slot shape [18, 21]. Slot antennas also have better isolation from the feed network and less interaction via

surface waves compared to patch antennas [6]. Also the effect of a finite ground plane on microstrip slot antennas is smaller than that of the microstrip patch antennas [42].

1.4 The Proposed Cavity Backed Slot Antenna

In this report we describe a novel slot antenna designed for wideband car-borne monopulse radars. A microstrip-fed cavity-backed slot (CBS) antenna is a slot radiator backed by a rectangular cavity and excited by a microstrip feed line. CBS antennas [12, 8, 24, 23] are promising candidates used in phased arrays, spacecraft, and wireless communication systems due to their compact size, high efficiency, and very small mutual coupling effect. Because of a slot cut in the ground plane, a microstrip line is free to radiate on both sides [40, 33]. A metallic cavity or a reflective wall is usually placed at the back of the slot to suppress the backward radiation when a unidirectional radiation pattern is required. This is a successful design for single slot element and wideband performance (about 35% impedance bandwidth for 10-dB return loss) has been demonstrated experimentally [18, 24]. In order to obtain this wideband property, the slot size, feed line location, and the cavity dimensions must be carefully chosen. This can be readily done for a single slot element, but for slot array applications this adjustment task will become prohibitively time consuming due to constraints on choosing the cavity dimension as well as the feed network. It has been shown that by using an inverted microstrip feed configuration, better radiation performance can be obtained [23, 22]. In this configuration, the metallic cavity is placed in the slot side to enhance the radiation in the side of the microstrip feed line. In other words, the substrate is now inverted. There are a number of advantages for this inverted arrangement [33]:

- Both theoretical and experimental studies on a microstrip-fed slot antenna showed that there is more radiated power in the microstrip feed line side hence providing more gain.
- The adjustment of cavity dimensions and changing the feed line location can be separately done since the feed network now is not placed inside the cavity. This adjustment flexibility can also give better antenna performance.
- It is easier and faster to simulate the inverted structure than the conventional one using Ansoft HFSS, thus making the design task a lot easier.

1.4.1 Use of Discrete Cavity Wall Backing

In order to avoid non-planar structural elements, vertical cavity walls are realized by discrete via holes, as inspired by [37, 38]. The discrete cavity suppresses the backward radiation and ensures that the antenna has a very low profile. It also enables the antenna to be fully planar and compatible with printed circuit fabrication process. Recently the technology of system-on-package (SOP) was developed. In system-on-package (SOP) it is desired to integrate antenna with RF circuits and systems together. This is made possible by the use of a discrete cavity which offers high Q-factors, high-integrations, low profile, low cost and mass-production.

1.5 Organization Of This Thesis

The thesis document is organized as follows:

- Chapter 1 gives the introduction of automotive based radars and the application of inverted cavity backed slot antennas in such radars.
- Chapter 2 describes the design of an inverted cavity backed slot antenna.
- Chapter 3 gives a brief description about simulation, fabrication methods, TRL calibration technique and practical pattern measurement method.

- Chapter 4 discusses both the simulation and measurement results for the cavity backed slot antenna design described in chapter 2.
- Chapter 5 gives a brief conclusion and scope for future work.

CHAPTER 2

CAVITY BACKED SLOT ANTENNA DESIGN

2.1 Introduction

In this chapter a detailed design description of our proposed inverted cavity backed slot antenna along is given along with photographs of the fabricated antenna model.

System design of the ultra-wide-band (UWB) car-borne radar system imposes the following requirements for the antennas.

1. Wide band: The antennas are required to transmit and receive short impulses covering frequency range [22 GHz, 29 GHz].
2. Low-cost: Since the car-borne radar sensors are intended for mass production, each sensor has to be cheap and easy to fabricate.
3. Compact, light-weight, and reliable. Because of size limit for each radar sensor, the antennas must be physically small, light, and mechanically reliable.

For initial study purposes an antenna prototype is simulated and measured around 3 GHz range as it is easier to control fabrication and measurement accuracies. The antenna design verified at 3 GHz range can be straightforwardly scaled to 24 GHz range. Printed patches are well known to be low-cost, compact, planar, and easy to fabricate, hence are always chosen as antennas for car-borne radars [17]. However, there exist a few disadvantages associated with patches. First, patches naturally have narrow bandwidth. Second, there exist mutual couplings among patch elements through the surface modes. And third, printed patches have considerable loss at sub-millimeter wave band. In this project, cavity-backed slots' are proposed

as array elements for the antennas on sensor nodes. Slot radiators are planar and conformal as patches. Their bandwidth can be as large as 40% by simply revising the slots' shapes [18]. The mutual couplings among elements are minimal because of the cavities' isolation; and the radiation performances are insensitive to the truncated ground plane [42]. Furthermore, slots' are more efficient than patches' since there is no dielectric loss.

2.2 Initial Design

2.2.1 Cavity Backed Loop Slot Antenna

The initial design of a cavity backed loop slot antenna is depicted in Figure 2.1. A slot loop is cut into a large perfect electrically conducting (PEC) plate and is backed by a square cavity made of PEC walls. The antenna is fed from the bottom of cavity by a coaxial feed and the inner co-axial conductor is extended into the cavity as an electric field excitation probe. The cavity dimensions are fixed to be 50 mm, 50 mm, and 13 mm along x, y, and z directions, respectively. Low-loss polyurethane foam is used as the material inside cavity. The antenna demonstrated more than 35% return loss.

2.2.2 Two Element Cavity Backed Loop Slot Antenna Array

The initial physical configuration for car-borne UWB antenna is depicted in Figure 2.1. In Figure 2.1, the element depicted is constructed into an array. The two elements of the array are physically identical to each other. The dimension of each of the elements of the antenna depicted in Figure 2.2 is same as the single element depicted in Figure 2.1. In each element, a slot loop is cut into a large perfect electrically conducting (PEC) plate and is backed by a square cavity. The cavity is made of PEC walls and filled with polyurethane foam (dielectric constant about 1.3).

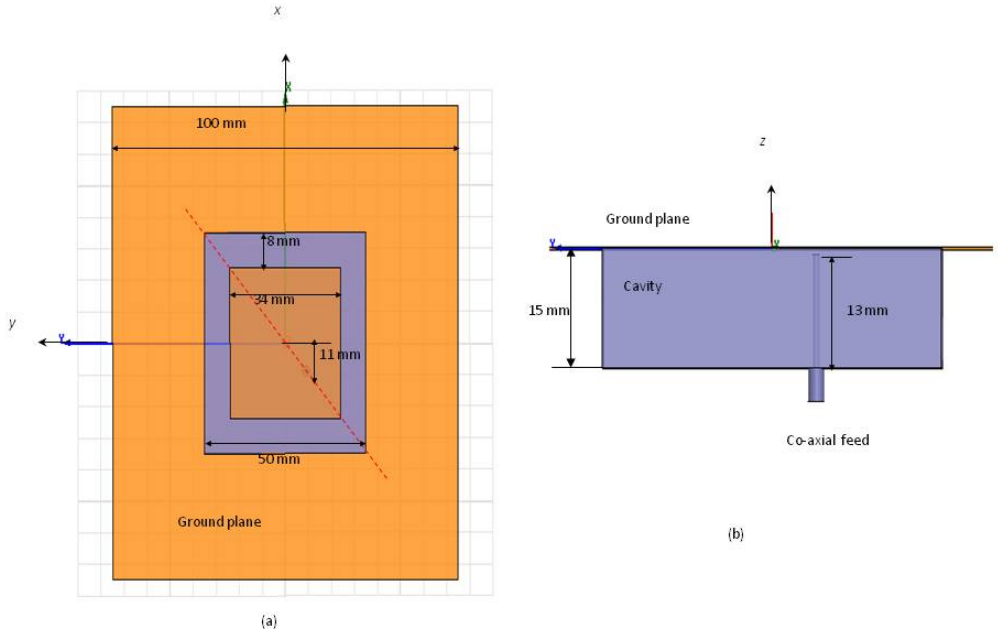

Figure 2.1. Cavity backed loop slot antenna (a) Top view, (b) Side view.

The separation is optimized to 60 mm so that coupling between the two elements is minimal. Each antenna element is fed from the bottom of its cavity by a coaxial cable and the inner co-axial conductor is extended into the cavity as an electric field excitation probe. The array element is matched to 50 ohm impedance from 3.8 GHz to 5.4 GHz, corresponding to about 35% relative bandwidth. Figure 2.3 shows a fabricated prototype of a two element cavity backed loop slot antenna.

In the above design high levels of side-lobes are observed from measured radiation patterns, which are due to large separation between the two elements. In order to suppress the side-lobes, we have improved the initial slot shape which was designed by a Doctoral Student Suman Kumar Gunnala from a loop to a rectangle. In this report, the loop design is termed initial design and the rectangle improved design.

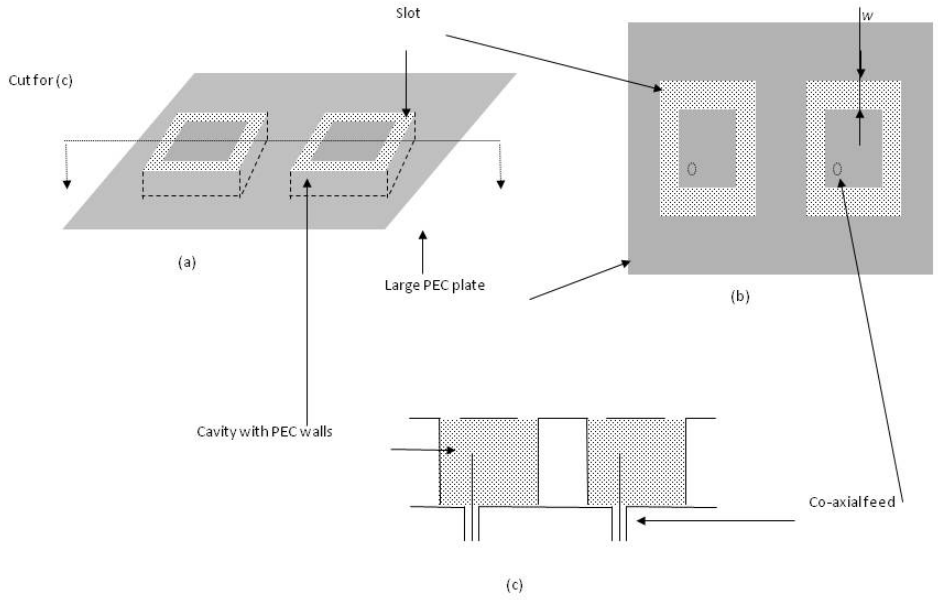

Figure 2.2. Loop CBS antenna array (a) Full view, (b) Top view, (c) Cut view.

2.3 Improved Design

2.3.1 Cavity Backed Rectangular Slot Antenna

In order to reduce element separation and in turn to suppress the side-lobes, a new rectangular slot shape was designed and a single element and two element array are designed and tested. The improved cavity backed slot antenna configuration is illustrated in the Figure 2.4. It consists of simple layered structures. The top layer is a double-clad printed circuit board; in our design, Rogers^{TM} 5880, with thickness 1.575 mm and dielectric constant 2.2, is used. A rectangular slot (20 mm by 60 mm) is etched on the bottom side of the circuit board as the radiating element. On the top side of the printed circuit board, there is a 50-ohm microstrip line to feed the slot. A dielectric slab resides underneath the slot, and its bottom is covered by a large ground

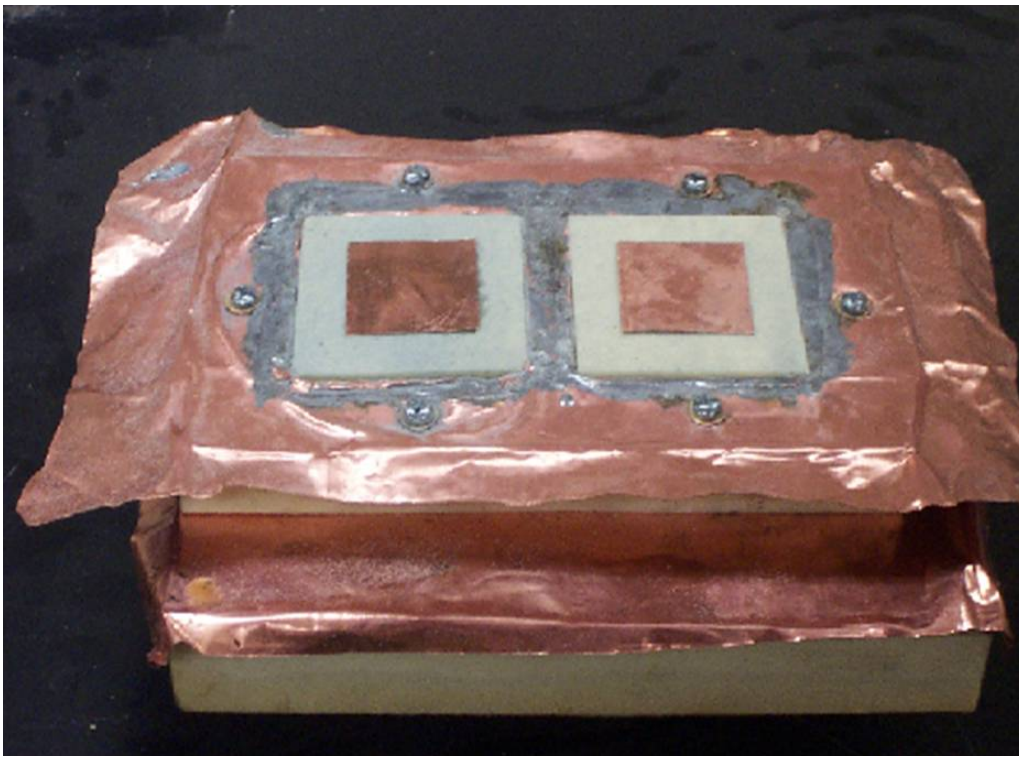

Figure 2.3. Fabricated prototype of cavity backed loop slot antenna array.

plane. The dielectric slabs' major functionality is to mechanically support multiple via holes connecting the bottom side of printed circuit board and the ground plane. The ground plane, bottom of the printed circuit board, and the vias jointly construct a cavity, which makes the slot radiation unidirectional and minimizes coupling among antenna elements in arrays. In our design, the dielectric slab is made of high density polyurethane foam, the vias have diameter 1 mm, and there are altogether 18 vias. The antenna in Figure 2.4 can be fabricated solely by printed circuit process, hence is robust, low-cost, and easy to integrate. A fabricated prototype is shown in Figure 2.5 and Figure 2.6.

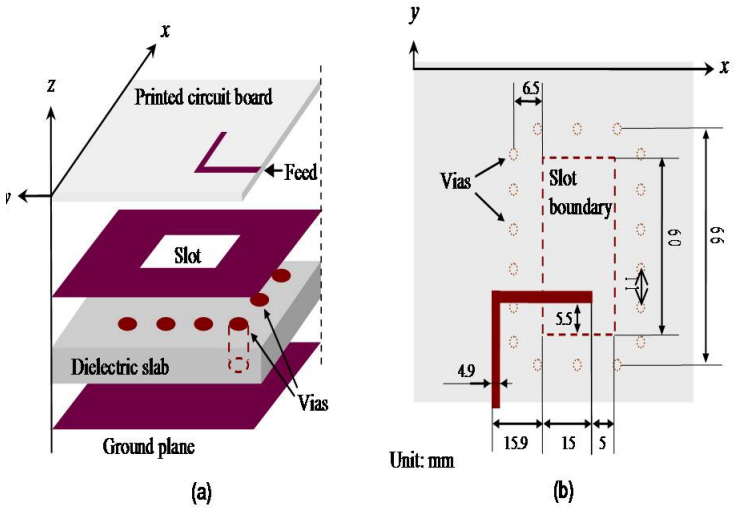

Figure 2.4. Inverted CBS antenna (a) Disassembled view, (b) Top view.

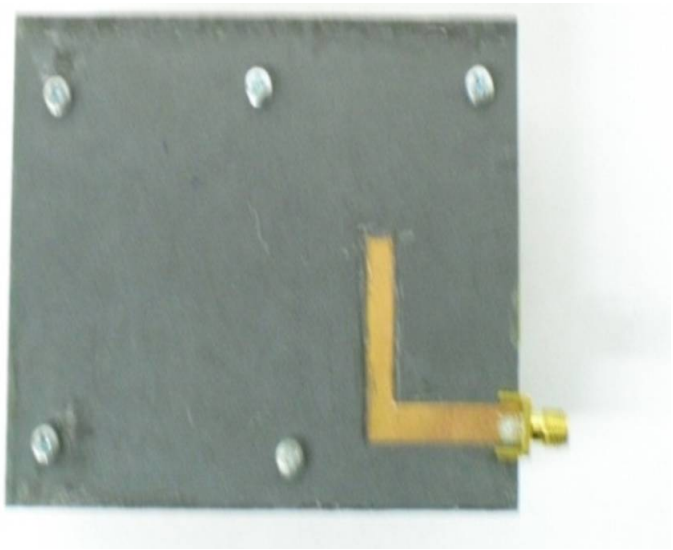

Figure 2.5. Fabricated inverted CBS antenna element front view.

2.3.2 Cavity Backed Rectangular Slot Antenna Array

The single element depicted in Figure 2.4 is constructed into a two element array. The two elements of the array are physically identical to each other. The dimension of each of the elements is same as the antenna depicted in Figure 2.4. In each element, a slot loop is cut into a large perfect electrically conducting (PEC)

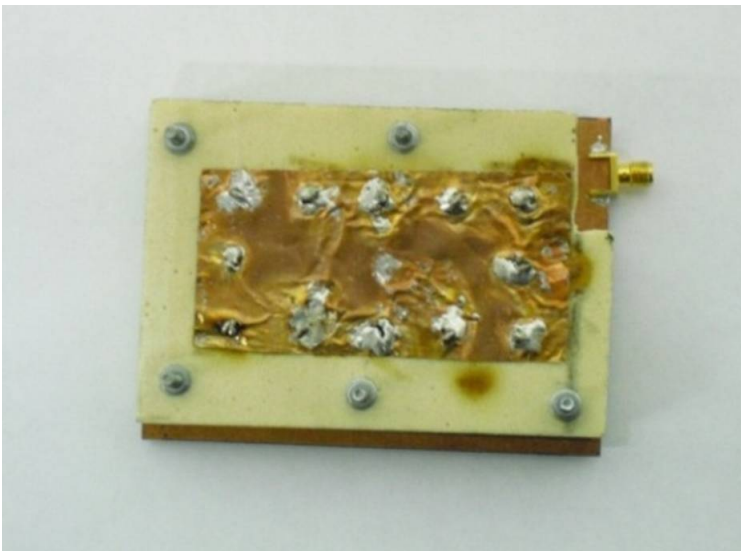

Figure 2.6. Fabricated inverted CBS antenna element bottom view.

plate and is backed by a rectangular cavity. The cavity is made of PEC walls and filled with polyurethane foam (dielectric constant about 1.3).

The separation is optimized to 50 mm so that coupling between the two elements is minimal. The printed circuit board at top layer makes use of Rogers^{TM} 5880 with thickness 1.575 mm and dielectric constant 2.2. Width of the microstrip feed line is designed to be 4.9 mm, which corresponds to 50 ohm characteristic impedance. High density polyurethane foam is chosen as the dielectric slab due to its low dielectric constant (between 1.3 and 1.8) and low loss. Signal delivery is realized by connecting a co-axial connector to the microstrip feed line. The impact of this co-axial connector is removed using standard thru-reflect-line (TRL) calibration [11]. Figure 2.7 and Figure 2.8 show the photo of a fabricated two-element array prototype front and bottom view respectively along with TRL calibration kits (two line kits are fabricated in order to accommodate the broad bandwidth of concern).

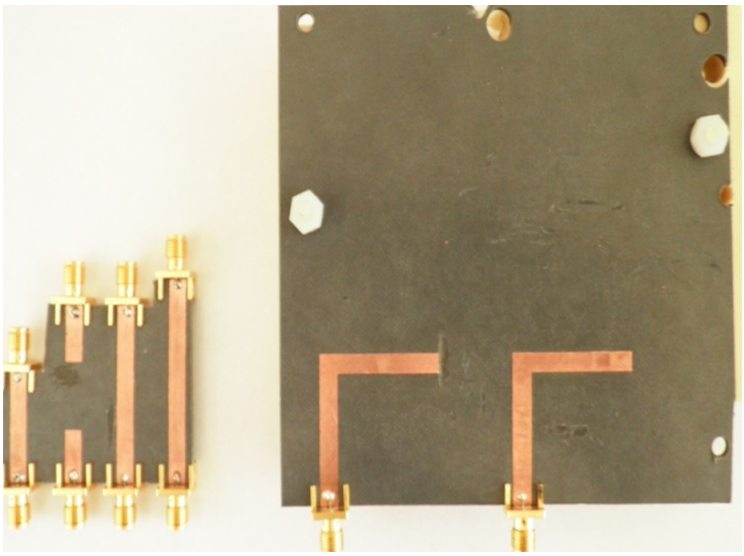

Figure 2.7. Prototype of inverted CBS antenna array front view.

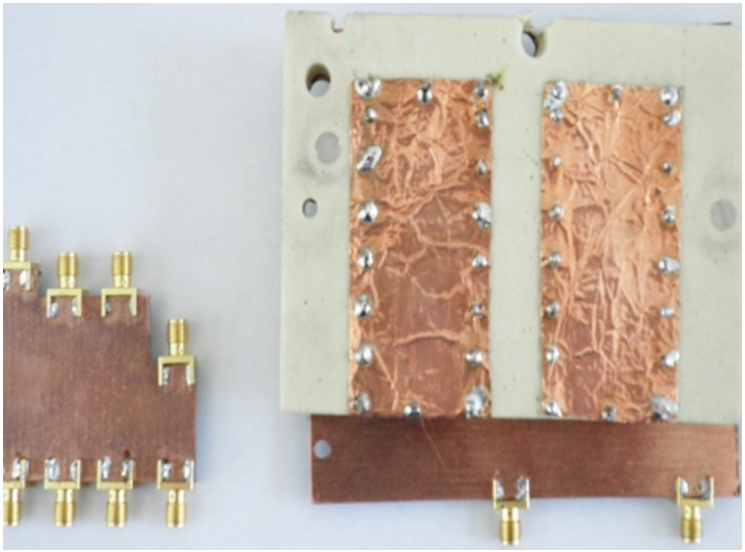

Figure 2.8. Prototype of inverted CBS antenna array bottom view.

CHAPTER 3

SIMULATION, CALIBRATION AND MEASUREMENT METHODS

3.1 Introduction

In this chapter, a description of the proposed cavity backed slot antenna design simulation is first given along with an explanation of the fabrication and practical pattern measurement techniques. The practical pattern measurement is carried out at the anechoic chamber of the University of Texas at Arlington. In addition a discussion on thru-reflect-line (TRL) calibration technique is also presented.

3.2 Simulation using Ansoft HFSS

Simulation of the improved cavity backed slot antenna design discussed in Chapter 2 is carried out using a 3-D full wave electromagnetic simulator Ansoft HFSS. Ansoft HFSS employs Finite Element Method (FEM) and adaptive meshing to solve 3-D Electromagnetic problems [35]. The detailed procedure adopted during simulation; creation of a 3-D model of the antenna and analysis is described in the section below. The design flow [35] is as shown in Figure 3.1.

3.2.1 3-D Cavity Backed Slot Antenna Model Development

The 3-D model of the cavity backed slot antenna is made up of several layers as shown in Figure 2.4. The modeling is done layer by layer starting from the bottom layer which is the ground plan all the way up to the top layer which comprised of a microstrip feed. Before component creation and material assignment, the solution type is set to Driven Terminal and the default units are set to mm. The default plane

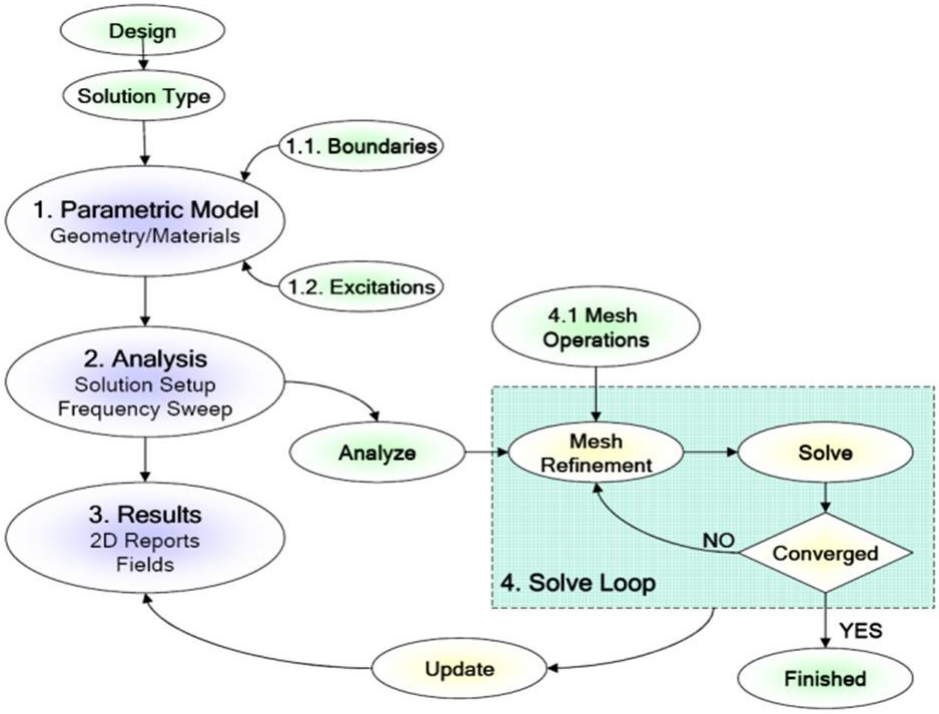

Figure 3.1. Design Flow in Ansoft HFSS [35].

is set to xy plane. The material used for each layer of the cavity backed slot antenna is given in Table 3.1. The material used for creating the discrete cavity i.e. foam is a user defined material with relative permittivity, (r=1.3) user defined. While creating the source as a lumped port, the resistance and full port impedance values are taken to be 50Ω.

Table 3.1. Model Development Summary

Component	Material
PCB	Rogers RT/Duroid 5880 (r=2.2)
Cavity	Foam (r=1.3)
Via Holes	Pec (r=1.0)
Feed	Perfect E
Ground	Perfect E
Source	Lumped Port
Air Box	Vaccum

The 3-D model for a single cavity backed slot antenna is shown in Figure 3.2 and a two element cavity backed slot antenna array is shown in Figure 3.3. The dimensions of both the single cavity backed slot antenna and two element cavity backed slot antenna array are as shown in Figure 2.4. In the two element cavity backed slot antenna array, both the elements are identical with the separation between them optimized to be one half the wavelength of centre frequency i.e. 50 mm.

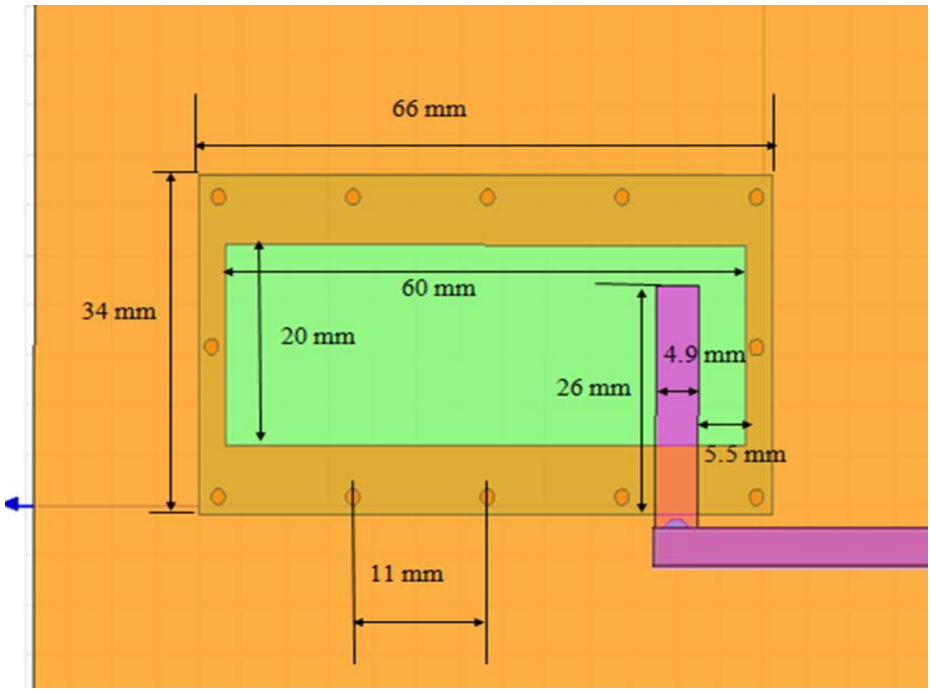

Figure 3.2. 3-D Model of cavity backed slot antenna element.

3.3 Fabrication Procedure

The fabrication procedure used to fabricate a practical prototype of the cavity backed slot antenna with centre frequency 3 GHz. However this method cannot be used when the antenna is scaled to 24 GHz range. A step-by-step fabrication procedure is given below:

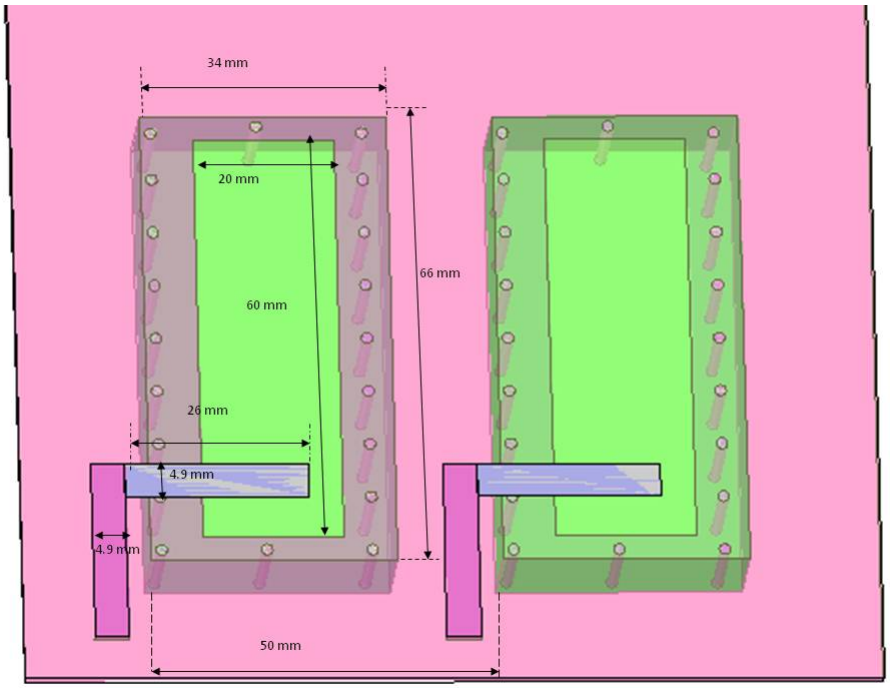

Figure 3.3. 3-D Model of two element cavity backed slot antenna array.

- Clean the board (copper) using alcohol.
- Warm up the laminator, set the temperature to 110 degree, and speed to 2. Just press the CARRI button. When the Ready light turns green, it means temperature is ok. If it flashes, it means the temperature is hotter.
- Turn off the light. All procedures involving photoresist must be done in a dark environment (This means there should be no ultraviolet light).
- Cut a piece of photoresist that is a bit larger than the board.
- There are 2 layers of plastic sheets, one among which is the photoresist. Peel off one layer a bit so that the other layer can cover back of the board.
- Wet the copper with water, but the board should not dribble drops. This is to make sure the photoresist is bonding to board steadily.
- Cover the board with photoresist from one end, and put the board into the laminator.

- Take off the peeled sheet while the board is rolled into.
- When the board comes out from the laminator, put it in the drawer (Dark place) 30 minutes to cool down.
- Press the COLD button on the laminator to cool down it. When the current temperature is below 60 cent degree (the roller stops), switch off the power.
- Place the mask on the laminated board and then place them under the UV lamp for exposure.
- Expose the laminated board under the UV lamp for 15 minutes.
- Keep the board in dark place for 15 minutes after exposure is complete.
- Combine developer fluid: one part pure developer and 10 parts water.
- Peel off another layer of a sheet from the board.
- Put the board in the developer for 40 to 50 seconds. Any longer than that, the exposed resist will be dissolve.
- Put the board in clean water. Scrape the photoresist with a scoop. The exposed resist should not be touched.
- Clean the board and dry it with paper. Do not touch the exposed resist. Put it in the drawer 15 minutes.
- Turn on the light. And warm up the iron. Set temperature gear to five.
- Put the board on the iron for 5 minutes to make the resist adhere to the board firmly. The color of resist will turn darker, maybe purple.
- Clean the board.
- Put the board in the etching chemical. The chemical is ready to use, needing no water. When doing this procedure, you should wear rubber gloves and respirator and blinders.

- Put the board in the chemical 40-50 minutes, and keep stirring the fluid. Time will be much shorter if the chemical is new. Usually the chemical should be replaced after 5 boards.
- Take the board out and put into clean water. After cleaning it with alcohol and water, put it in the developer again. Time taken to dissolve the resist is much longer.
- Clean it and the fabricated board is ready.

3.4 Pattern Measurement Methods

The pattern of the single cavity backed slot antenna and the two element cavity backed slot antenna array described in Chapter 2 are measured in the anechoic chamber at University of Texas at Arlington. The radiation patterns i.e. amplitude and phase, polarization, and gain of an antenna which are used to characterize its radiation capabilities, are measured on the surface of a constant radius sphere shown in Figure 3.4. Due to there being a fixed radial distance the only the two angular co-ordinates (Θ and Φ) are needed for positional identification. A representation of the radiation characteristics of the radiator as a function of Θ and Φ for a constant radial distance and frequency is defined as the pattern of the antenna. A three dimensional pattern is generally constructed by a number of two dimensional patterns. The number of two dimensional patterns required depends on the functional requirements of the given description. In general the orthogonal principle E-plane and H-plane patterns are sufficient to construct a three dimensional pattern. A two dimensional pattern is a pattern cut and is obtained by fixing one of (Θ and Φ) while varying the other. If Θ is fixed ($0 \leq \Theta_i \leq \Pi$) and Φ is varied ($0 \leq \Phi_i \leq 2\Pi$) then the pattern obtained is called azimuthal pattern, which is presented in Chapter 4 for the cavity backed slot radiator designed. If Φ is fixed ($0 \leq \Phi_i \leq \Pi$) and Θ is varied

($0 \leq \Theta_i \leq 2\Pi$) then the pattern obtained is called elevation pattern. The radiation patterns can be measured in the transmitting or receiving mode depending on the application and type of antenna. As the cavity backed slot antenna described in this report is reciprocal, it can either be measured in transmitting or receiving modes.

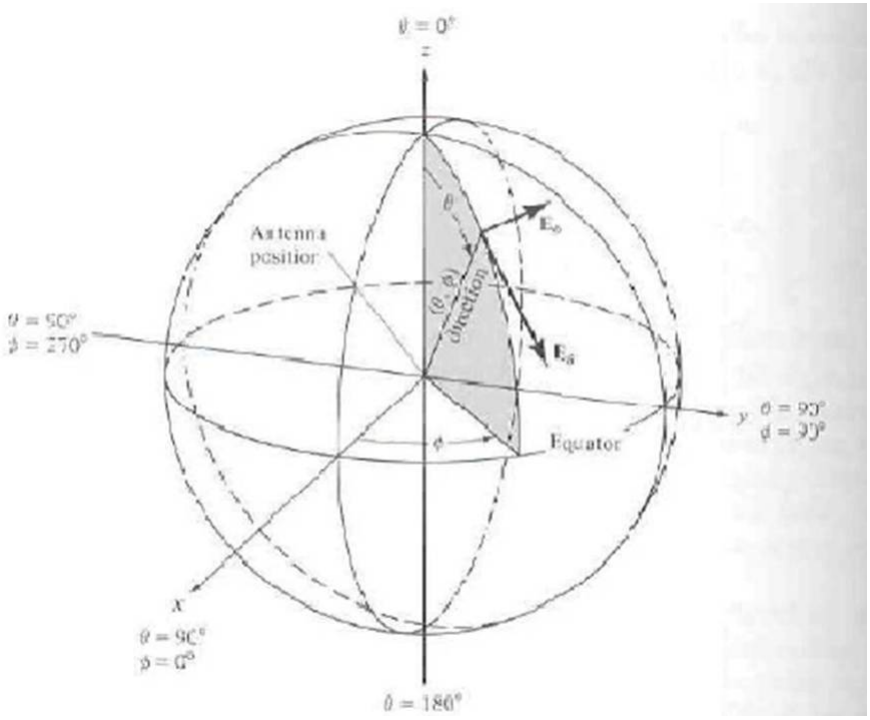

Figure 3.4. Antenna pattern measurement co-ordinate system [7].

The antenna range instrumentation is generally classified into five categories:

1. Source antenna and transmitting system.
2. Receiving system.
3. Positioning system.
4. Recording system.
5. Data-processing system.

Figure 3.5 shows a typical arrangement of an antenna range instrumentation setup.

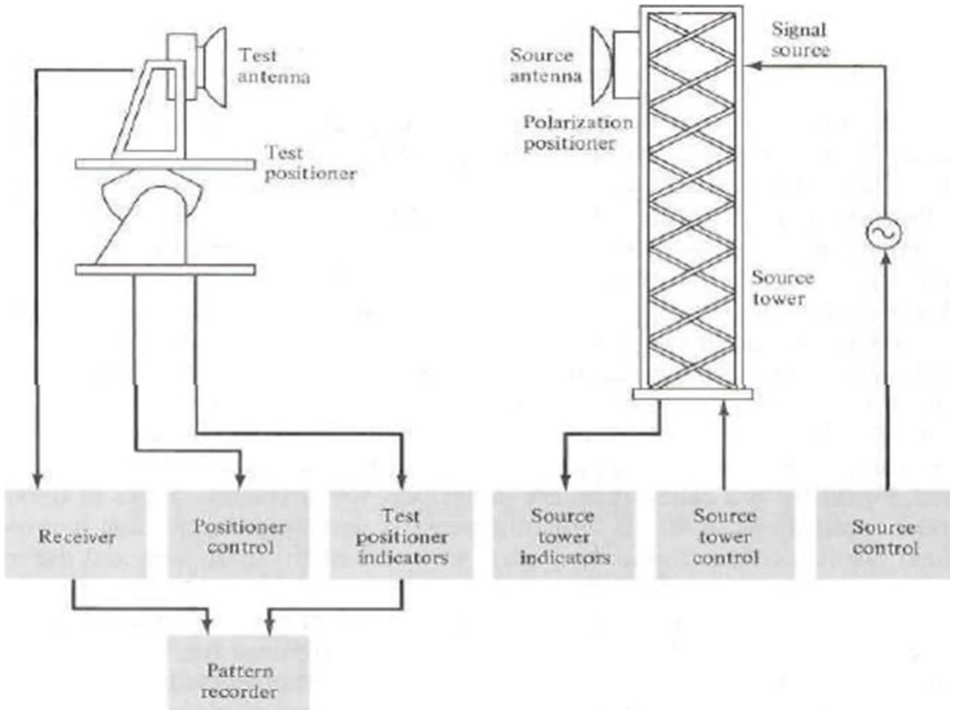

Figure 3.5. Instrumentation for an antenna range measurement system [7].

In our measurement setup, the pattern measurements are performed in an indoor range (anechoic chamber) with the source antenna being a Horn and the test antenna being the cavity backed slot radiator. A HP 8510C Vector Network Analyzer (VNA) is used to record the measured data. The entire pattern is measured by rotating the turn table on which the test antenna is mounted over 0^0 to 360^0 in steps of 5^0. The entire process is automated using Lab View which collects the data from the VNA and then proceeds to rotate the turn table before measuring the next data set.

3.5 Three Antenna Method

Measurement is carried out in our anechoic chamber, with the two steps:

- A horn-to-horn configuration is measured, using two standard gain horn antennas. The horns' gain can be found from the following formulation,

$$P_r = P_t * (G_t * G_r) * (\lambda/4 * \Pi * r) \tag{3.1}$$

  In the above, P_t and P_r are transmitted and received powers respectively, G_t and G_r are gains of transmitted and receiving antennas respectively, R is the distance between transmitting and receiving antennas, and λ is wavelength. Ratio between P_r and P_t is given by S_{21} with the aid of thru calibration. When G_t and G_r are assumed identical, they can be straightforwardly calculated.
- One of the horns in the above step is replaced by both the single element cavity backed antenna and the two-element array. Gain of both the antennas is then found through comparison with the horn-to-horn data.

3.5.1 Monopulse Beam Scanning

For the two element cavity backed slot antenna array, to achieve monopulse beam-scanning, the two elements are fed by same magnitude but different phase according to the configuration in Figure 3.6 . Input power is split into half to feed the two elements. A time-delay cell is inserted in between an element and power splitter, to adjust the timing difference between the two elements. In our experiments, the time-delay cell is made of co-axial transmission lines.

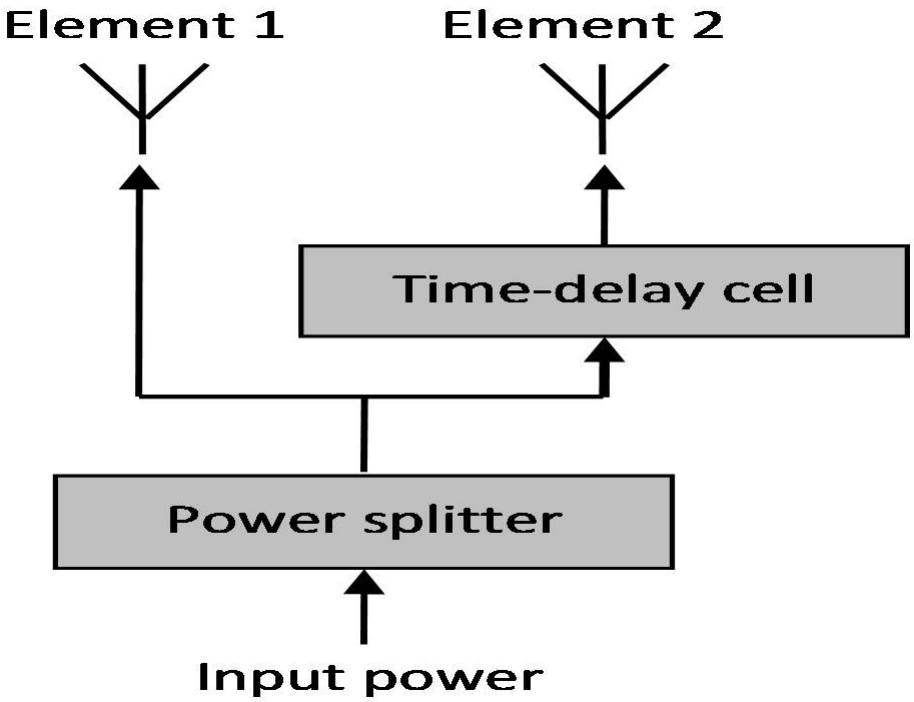

Figure 3.6. Feed structure of the two-element array.

3.6 TRL Calibration

In our design the signal delivery is realized by connecting a co-axial connector to the microstrip feed line. In order to remove the effect of this connector, a TRL calibration kit has been designed and fabricated. In order to accommodate the wide bandwidth of the cavity backed slot antenna two lines are designed at 2.5 GHz and 3.5 GHz respectively. The equations used to design the line length and de-embedding of DUT are given below.

3.6.1 Line Length Design

Two separate line lengths at 2.5 GHz and 3.5 GHz are designed in order to accommodate the wide bandwidth of our antenna. The design procedure is as given below:

- The effective di-electric constant of air and PCB is calculated using the following formulation,

$$\epsilon_{reff} = ((\epsilon_r + 1)/2) + ((\epsilon_r - 1)/2) * (1 + (12 * h/w)) \tag{3.2}$$

where r is the di-electric constant of PCB material (2.2), h is the thickness of slot and w is the slot width.

- The phase velocity is then calculated using the formulation,

$$V_p = c/\epsilon_{reff} \tag{3.3}$$

where c is a constant ($3*10^8$).

- The line length is calculated using,

$$\beta * l = \Pi/2 \tag{3.4}$$

and,

$$\beta = 2 * \Pi/\lambda \tag{3.5}$$

and,

$$\beta = 2 * \Pi/\lambda \tag{3.6}$$

λ is the wavelength ($\lambda = V_p$/frequency)

3.6.2 De-embedding of DUT

The equations used in the Matlab code for de-embedding the effect of the co-axial connector in all the cavity backed slot antenna designs are as given below.

The modelling of a thru in TRL is as shown below. The S parameter matrix for thru is,

$$\overline{S_T} = \begin{bmatrix} (S_{11})_T & (S_{11})_T \\ (S_{11})_T & (S_{11})_T \end{bmatrix}$$

The S-Parameter matrix will be transformed into the wave cascading matrix R as follows,

$$\overline{S_T} \rightarrow \overline{R_T} \;\; \overline{S_A} \rightarrow \overline{R_A} \;\; \overline{S_B} \rightarrow \overline{R_B}$$

The relationship between $\overline{R_T}$, $\overline{R_A}$ and $\overline{R_B}$ is given by,

$$\overline{R_T} = \overline{R_A} \;\; \overline{R_B} \tag{3.7}$$

In the model for reflection two values w_1 and w_2 are measured and in terms of scatter parameters w1 and w2 are given as,

$$w_1 = (S_{11})_A + (S_{12})_A S_{21})_A \Gamma_R / 1 - S_{22})_A \Gamma_R \tag{3.8}$$

$$w_2 = (S_{22})_B + (S_{21})_B S_{12})_B \Gamma_R / 1 - S_{11})_B \Gamma_R \tag{3.9}$$

In terms of wave cascading matrix parameters w1 and w2 are given as,

$$w_1 = (R_{12})_A + (R_{11})_A \Gamma_R / R_{22})_A + R_{21})_A \Gamma_R \tag{3.10}$$

$$w_2 = (R_{11})_B \Gamma_R - (R_{21})_B / R_{22})_B - R_{12})_B \Gamma_R \tag{3.11}$$

The modelling of a line in TRL is as shown below. The S parameter matrix for line is,

$$\overline{S_D} = \begin{bmatrix} (S_{11})_D & (S_{11})_D \\ (S_{11})_D & (S_{11})_D \end{bmatrix}$$

The S-Parameter matrix will be transformed into the wave cascading matrix R as follows,

$$\overline{S_D} \rightarrow \overline{R_D} \;\; \overline{S_A} \rightarrow \overline{R_A} \;\; \overline{S_B} \rightarrow \overline{R_B}$$

The relationship between $\overline{R_D}$, $\overline{R_A}$ and $\overline{R_B}$ is given by,

$$\overline{R_D} = \overline{R_A} \;\; \overline{R_L} \;\; \overline{R_B} \tag{3.12}$$

CHAPTER 4

RESULTS AND DISCUSSION

4.1 Introduction

In this chapter, some simulation and measurement results are presented to demonstrate the performance of the inverted cavity backed slot (CBS) antenna and two element inverted cavity backed slot antenna array.

4.2 CBS Element Results

The imput impedance result and broadside pattern measurement results for an inverted cavity backed slot antenna element are presented in this section.

4.2.1 Single Element Input Impedance Result

The simulated and measured S_{11} data for the improved design inverted cavity backed slot antenna element are plotted in Figure 4.1.

As seen in Figure 4.1, the input impedance bandwidth is about 30.5% and the simulation and measurement results are in excellent aggrement with each other.

4.2.2 Single Element Pattern Measurement Results

The pattern results for an inverted cavity backed slot antenna element at different frequencies (2.8 GHz, 2.9 GHz, 3 GHz, 3.1 GHz and 3.2 GHz) are shown in Figure 4.2 to Figure 4.6. As seen in Figure 4.2 to Figure 4.6, the broadside pattern gain is about 6.0 dBi for both the measured case as well as simulated case.

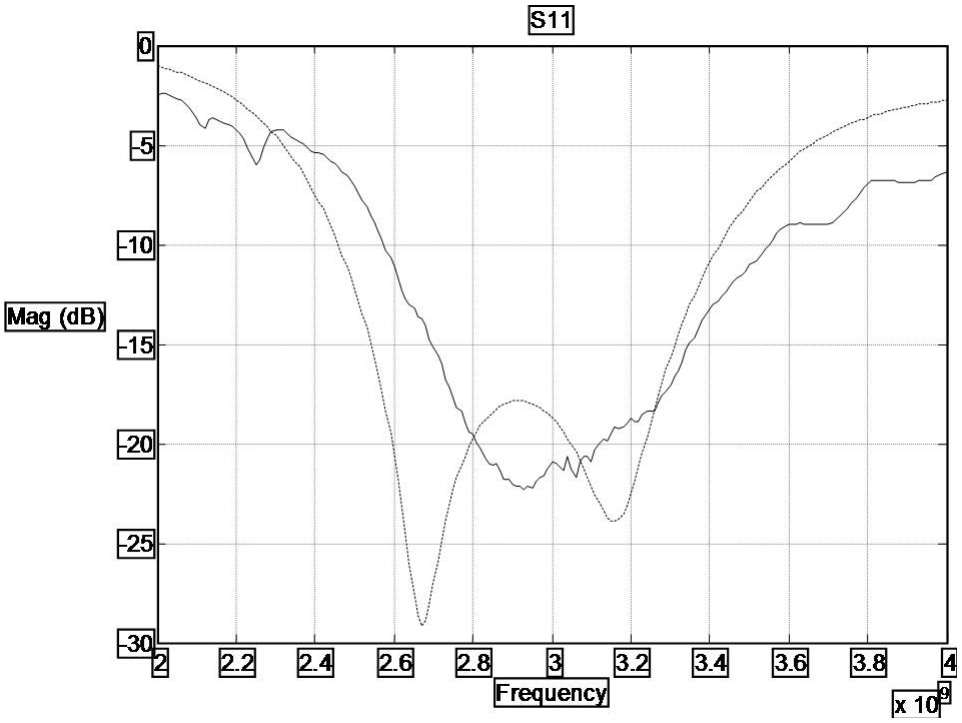

Figure 4.1. Input impedance of inverted cavity backed slot antenna element.

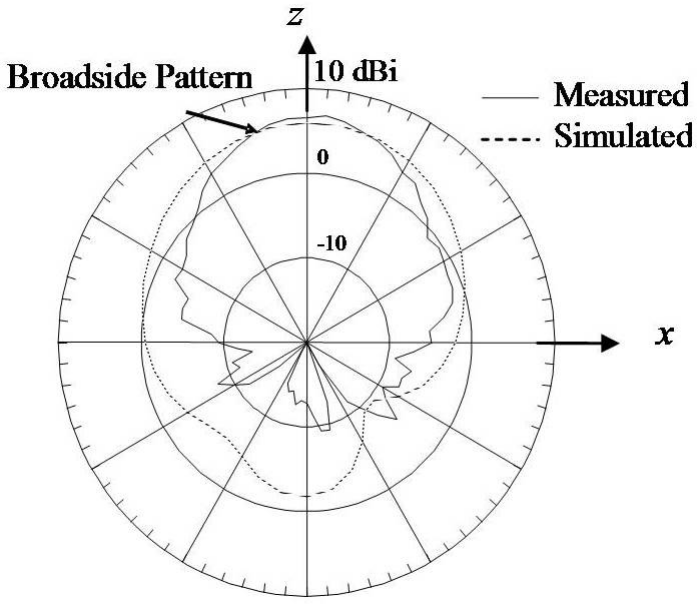

Figure 4.2. Broadside radiation pattern at 2.8 GHz.

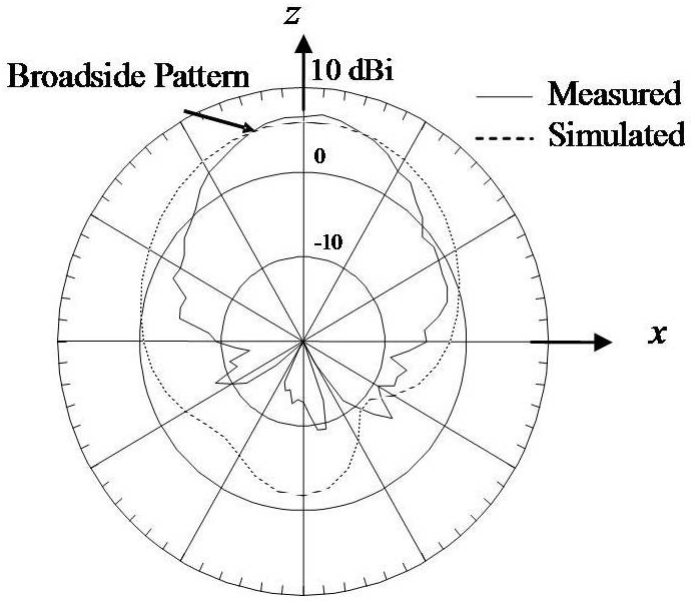

Figure 4.3. Broadside radiation pattern at 2.9 GHz.

4.3 Two Element Array Results

The input impedance results and broadside pattern measurement results for a two element inverted cavity backed slot antenna array are presented in this section.

4.3.1 Two Element Array Input Impedance Results

The simulated and measured S_{11} data of both elements of an inverted cavity backed slot antenna array are plotted in Figure 4.7 and Figure 4.8.

As seen in Figure 4.7 and Figure 4.8, the operating frequency band for the array is from 2.61 GHz to 3.44 GHz which corresponds to an input impedance bandwidth of about 27.5%. The simulation and measurement results are in excellent aggrement with each other. The operating frequency band for the array is from 2.61 GHz to 3.44 GHz.

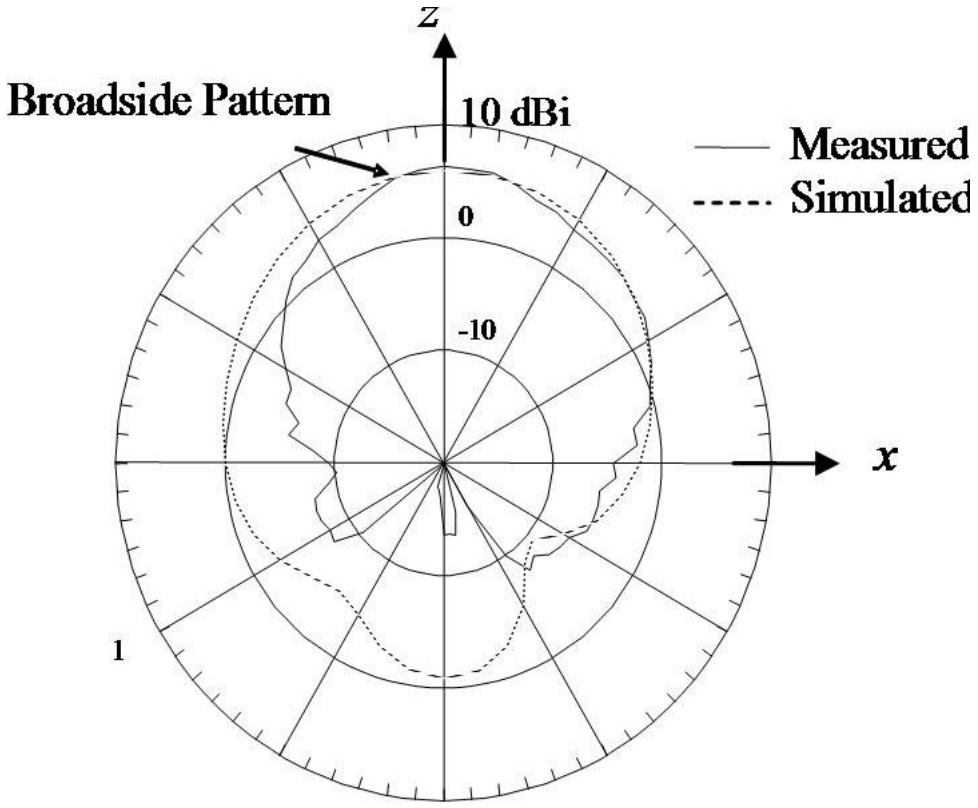

Figure 4.4. Broadside radiation pattern at 3.0 GHz.

4.3.2 Two Element Array Forward Pattern Results

The forward pattern results for an inverted cavity backed slot antenna element at different frequencies (2.8 GHz, 2.9 GHz, 3 GHz, 3.1 GHz and 3.2 GHz) are shown in Figure 4.9 to Figure 4.14.

As seen in Figure 4.9 to Figure 4.14, the simulated and measured forward null pattern are in excellent agreement with each other. The simulated gain is around 9 dBi while the measured gain is around 8 dBi. The difference of 1 dBi is due to the practical losses during measurement in the anechoic chamber. The phase difference between the phase shifters during this measurement is 0^0.

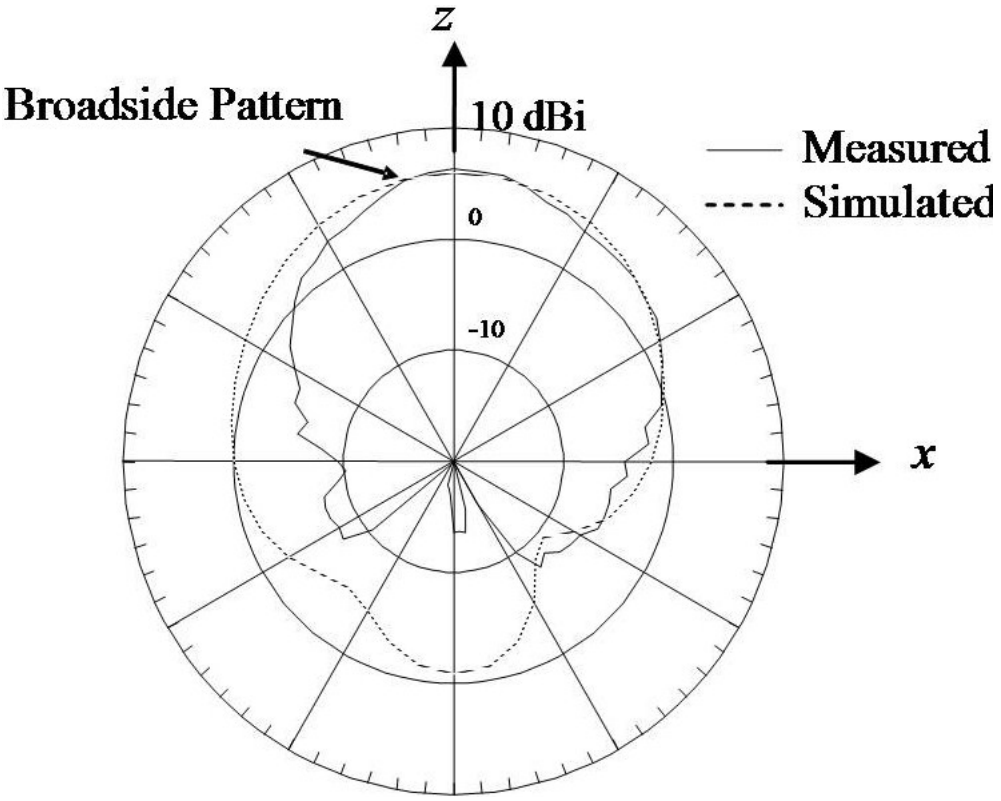

Figure 4.5. Broadside radiation pattern at 3.1 GHz.

4.3.3 Two Element Array Forward Null Pattern Results

The forward null pattern results for an inverted cavity backed slot antenna element at different frequencies (2.8 GHz, 3 GHz and 3.2 GHz) are shown in Figure 4.15 to Figure 4.17.

As seen in Figure 4.15 to Figure 4.17, the simulated and measured forward null pattern are in excellent agreement with each other. The simulated gain is around 7 dBi while the measured gain is around 6 dBi. The difference of 1 dBi is due to the practical losses during measurement in the anechoic chamber. The phase difference between the phase shifters during this measurement is 180^0.

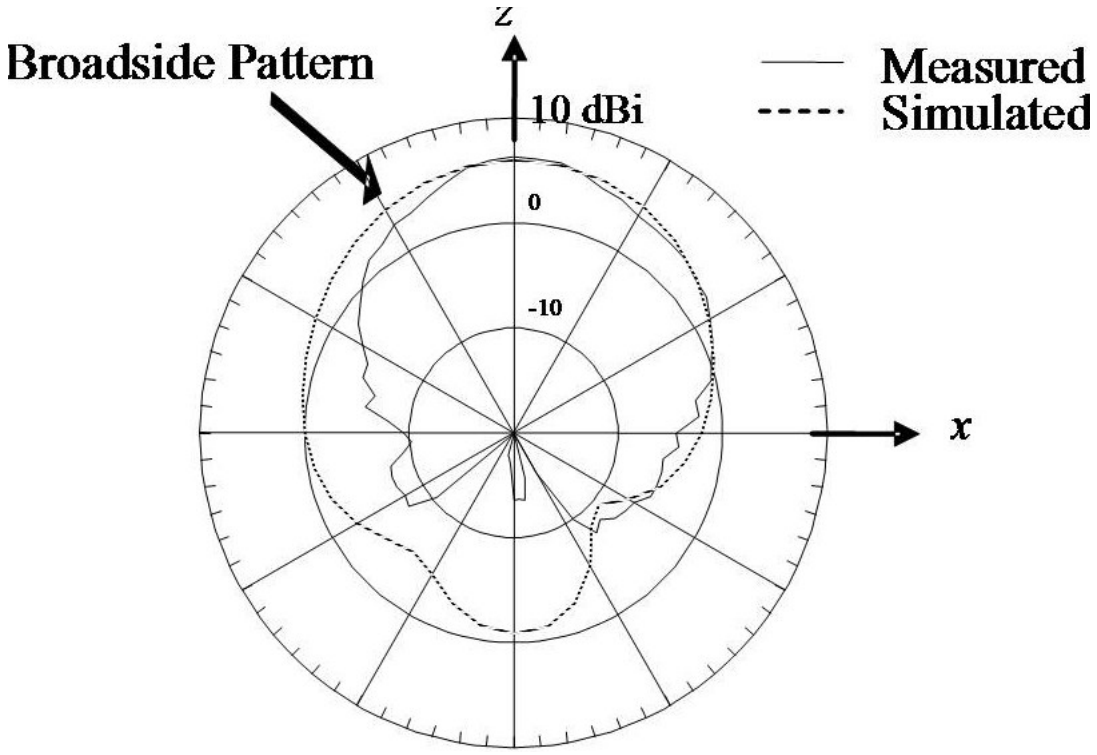

Figure 4.6. Broadside radiation pattern at 3.2 GHz.

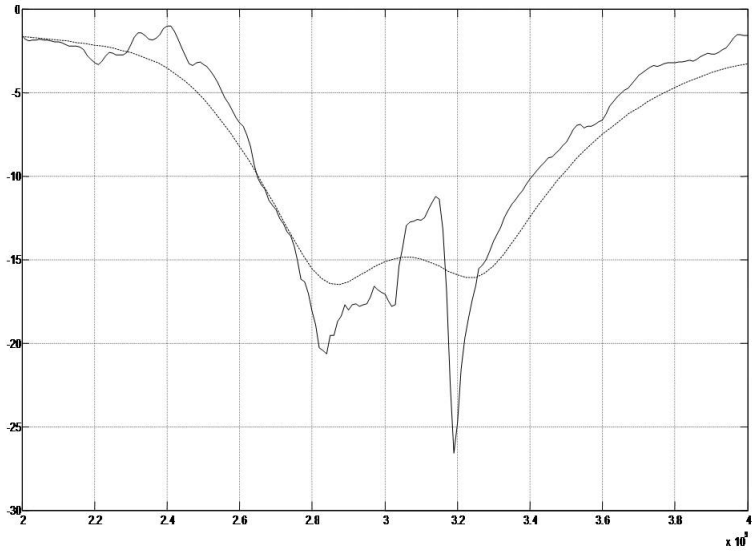

Figure 4.7. Input impedance of inverted cavity backed slot antenna element.

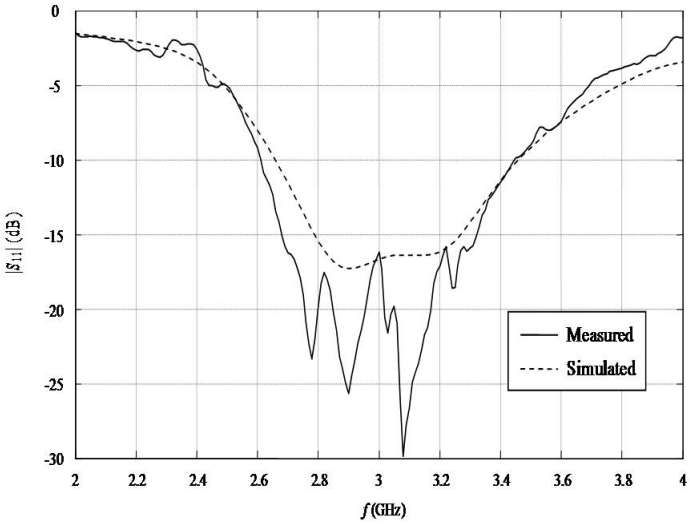

Figure 4.8. Input impedance of inverted cavity backed slot antenna element.

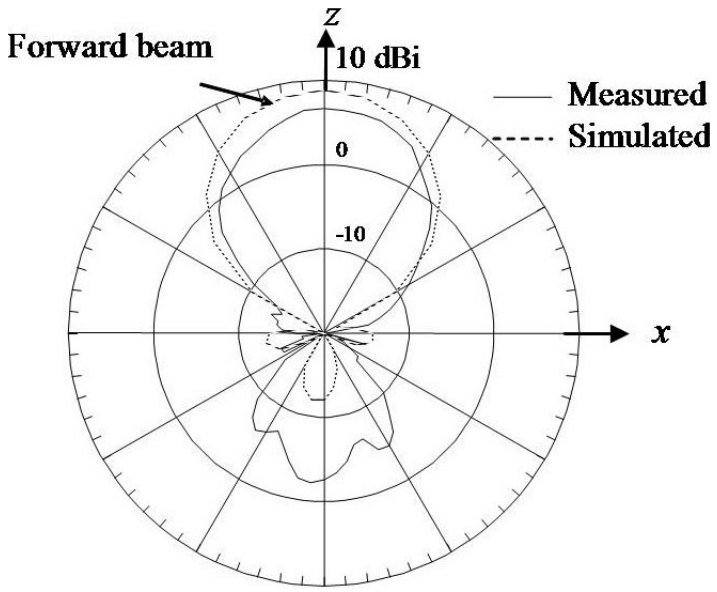

Figure 4.9. Broadside forward radiation pattern at 2.8 GHz.

4.3.4 Two Element Array Beamscan Pattern Results

The beamscan pattern results for an inverted cavity backed slot antenna element at different frequencies (3 GHz, 3.1 GHz and 3.2 GHz) are shown in Figure 4.18 to Figure 4.20.

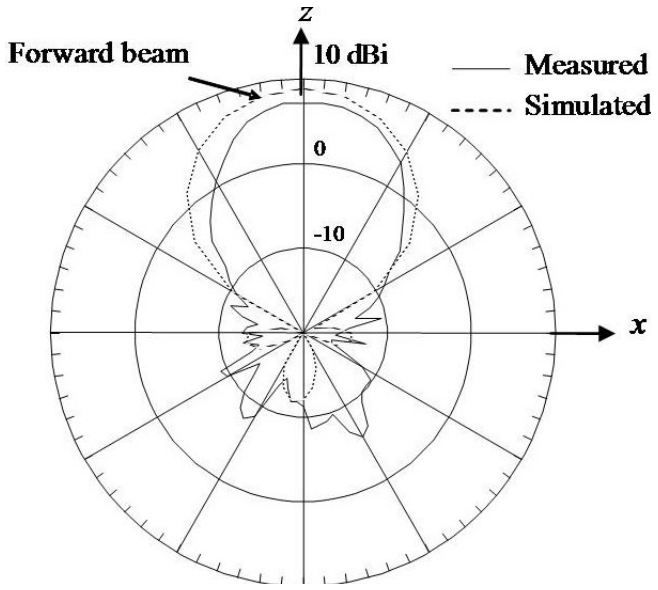

Figure 4.10. Broadside forward radiation pattern at 2.9 GHz.

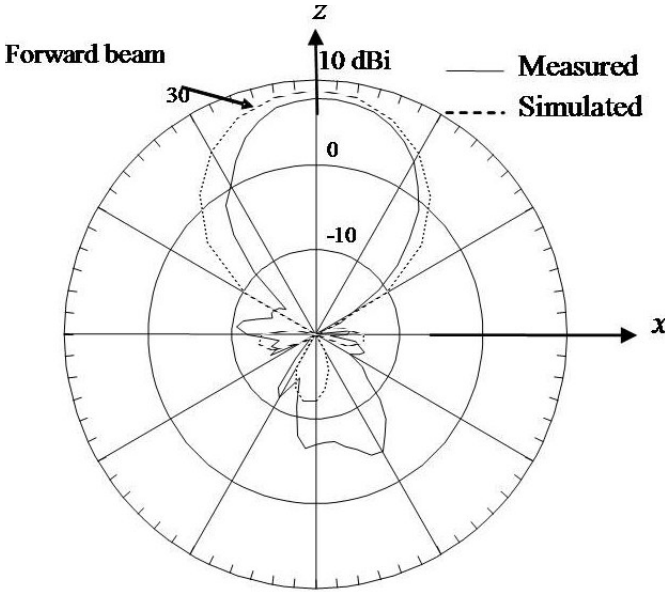

Figure 4.11. Broadside forward radiation pattern at 3.0 GHz.

As seen in Figure 4.18 to Figure 4.20, the simulated and measured forward null pattern are in excellent agreement with each other. The simulated gain is around 8.5 dBi while the measured gain is around 7.5 dBi. The difference of 1 dBi is due to the

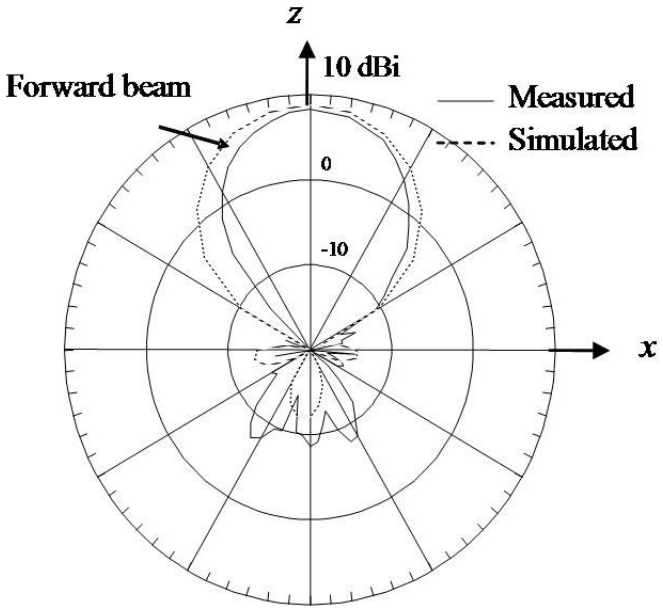

Figure 4.12. Broadside forward radiation pattern at 3.1 GHz.

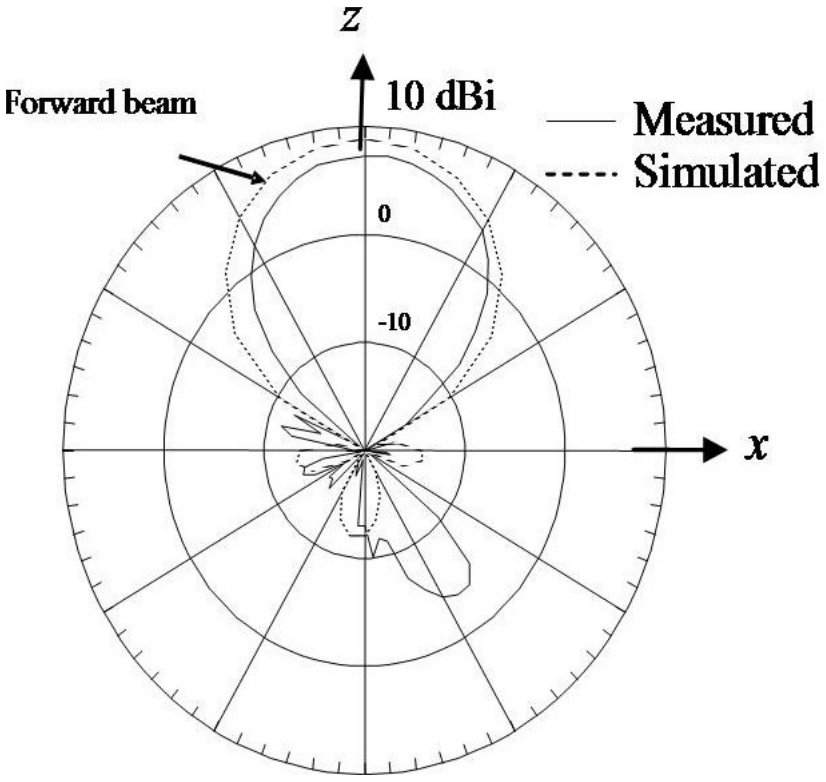

Figure 4.13. Broadside forward radiation pattern at 3.2 GHz.

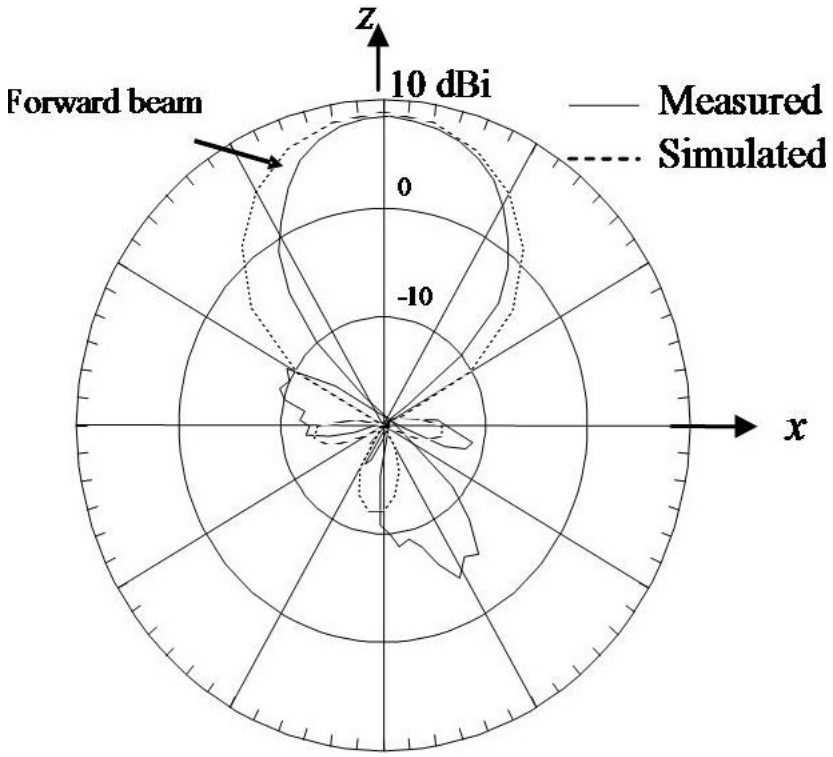

Figure 4.14. Broadside forward radiation pattern at 3.3 GHz.

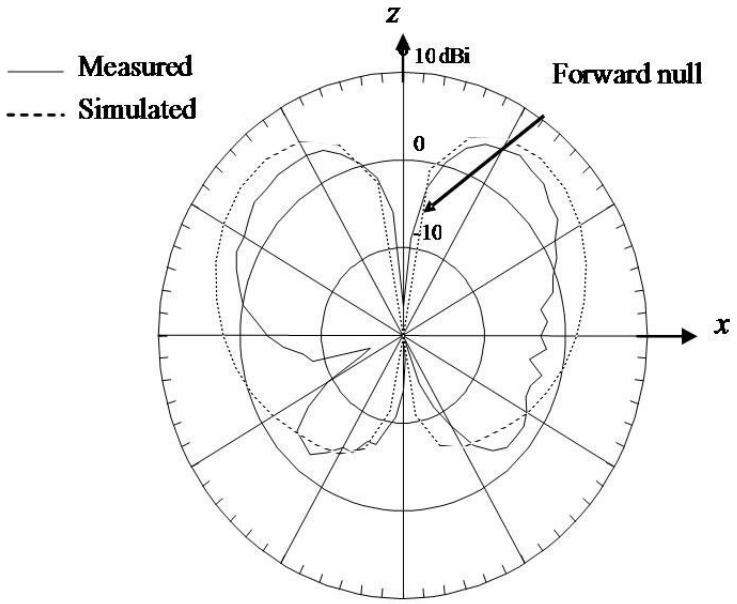

Figure 4.15. Broadside forward null radiation pattern at 2.8 GHz.

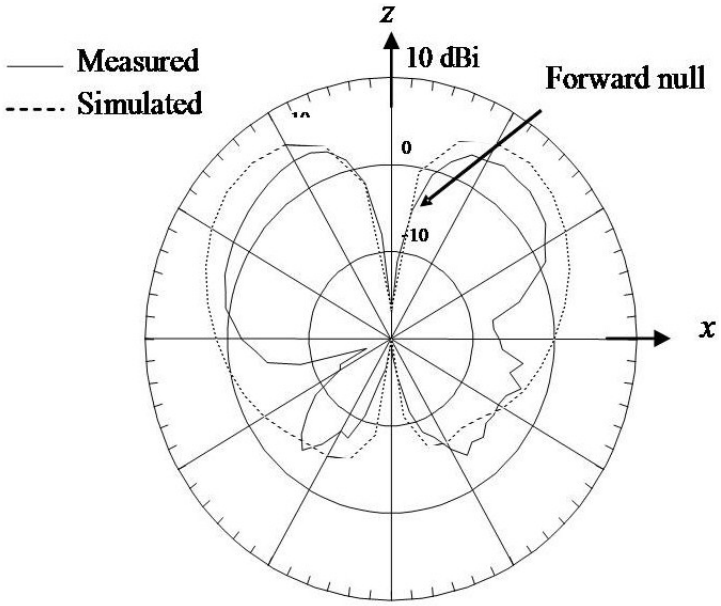

Figure 4.16. Broadside forward null radiation pattern at 3.0 GHz.

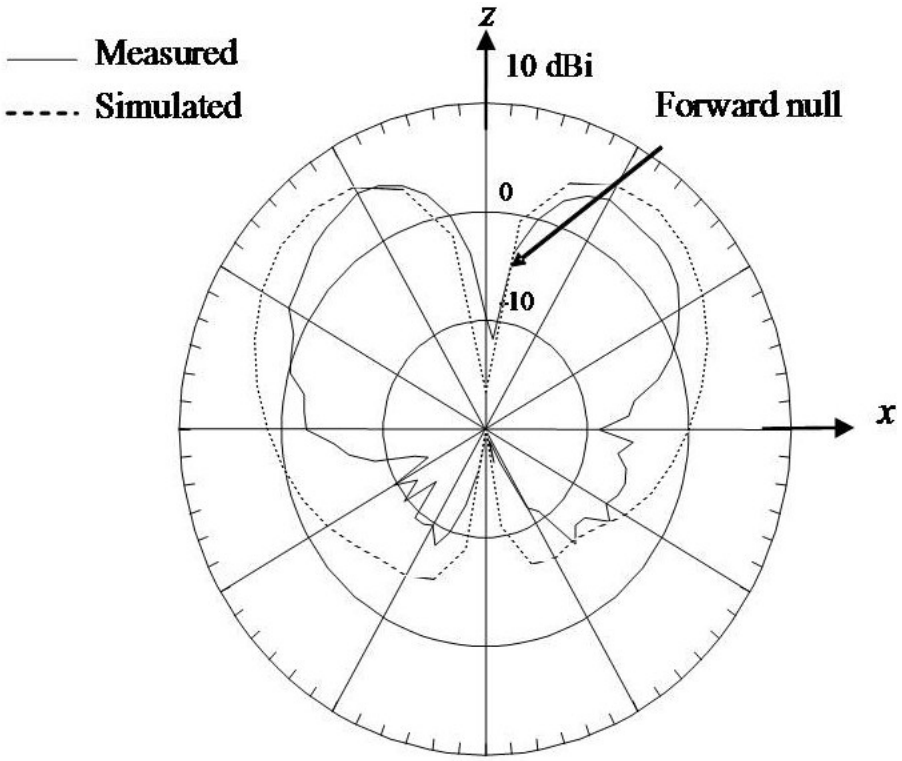

Figure 4.17. Broadside forward null radiation pattern at 3.2 GHz.

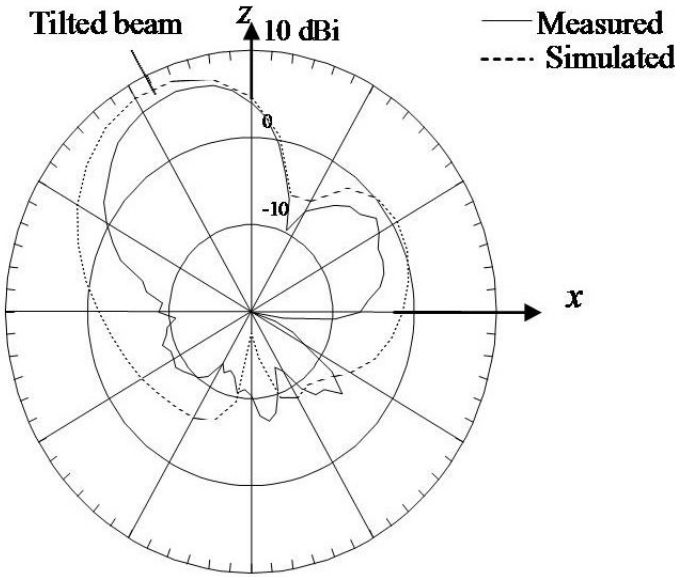

Figure 4.18. Broadside beamscan radiation pattern at 3.0 GHz.

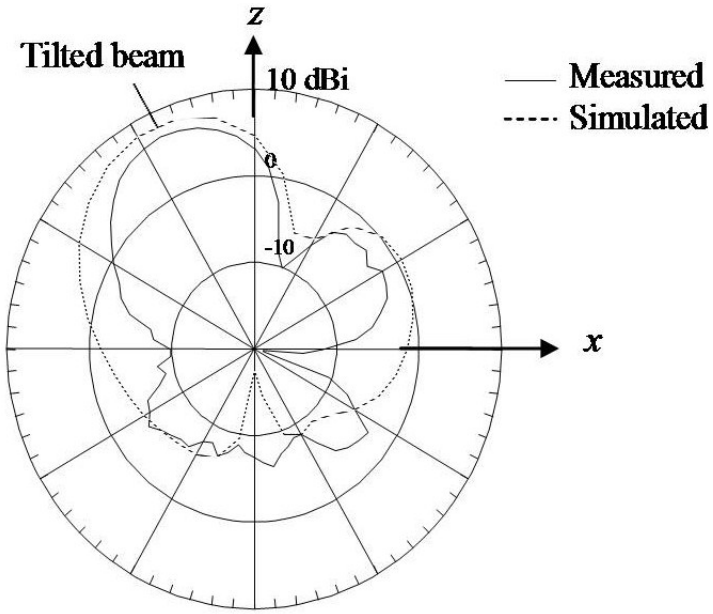

Figure 4.19. Broadside beamscan radiation pattern at 3.1 GHz.

practical losses during measurement in the anechoic chamber. The phase difference between the phase shifters during this measurement is 80^0.

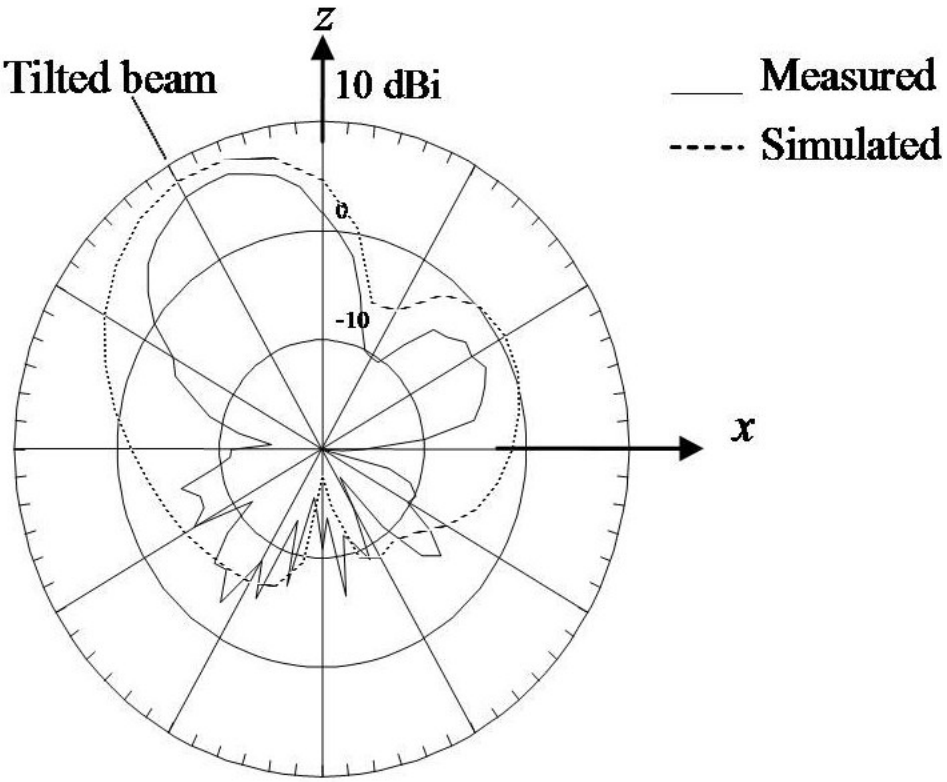

Figure 4.20. Broadside beamscan radiation pattern at 3.2 GHz.

4.3.5 Two Element Array Beamscan Null Pattern Results

The beamscan null pattern results for an inverted cavity backed slot antenna element at different frequencies (3 GHz and 3.2 GHz) are shown in Figure 4.21 to Figure 4.22.

As seen in Figure 4.21 to Figure 4.22, the simulated and measured forward null pattern are in excellent agreement with each other. The simulated gain is around 8.5 dBi while the measured gain is around 7.5 dBi. The difference of 1 dBi is due to the practical losses during measurement in the anechoic chamber. The phase difference between the phase shifters during this measurement is 260^0.

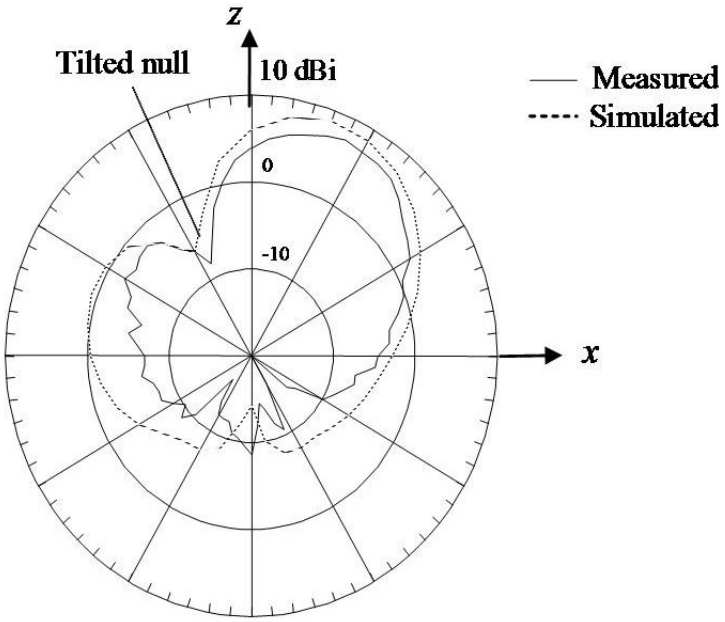

Figure 4.21. Broadside beamscan null radiation pattern at 3.0 GHz.

4.4 Results Overview

Ansoft HFSS^{TM} is used for antenna simulation, and both the single element and the two-element array are measured at the anechoic chamber of the University of Texas at Arlington. Input impedance characteristics of the single element is shwon in Figure 4.1. Input impedance characteristics of the two antenna elements of the array are very similar as shown in Figure 4.7 and Figure 4.8. The simulated and measured data have excellent agreement. If -10 dB is used as the matching criterion, the fabricated antenna has operating frequency band [2.61 GHz, 3.44 GHz], which corresponds to 27.5% fractional bandwidth. Both the single element and two element array shows stable radiation behaviour throughout the matching band. Results for both antenna are plotted in this chapter. Monopulse beam-scanning results are plotted in this section. To achieve monopulse beam-scanning, the two elements are fed by the same magnitude but different phases. The radiation patterns in this section are obtained at different frequencies, when the phase differences between the two antenna

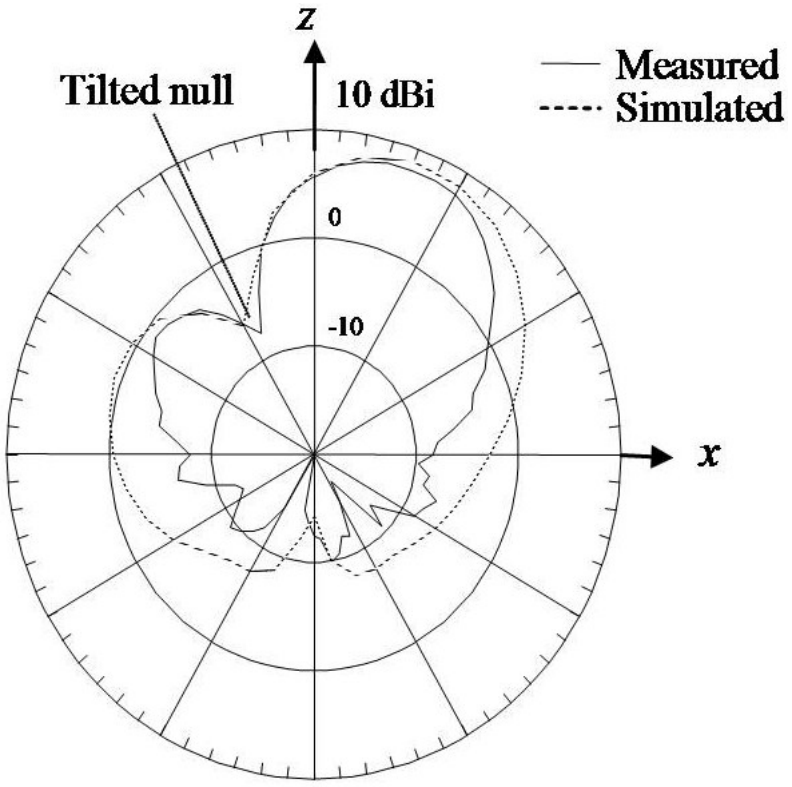

Figure 4.22. Broadside beamscan null radiation pattern at 3.2 GHz.

elements are 0^0, 180^0, 80^0 and 260^0 respectively. Simulation and measurement match each other very well. When the phase difference is 0^0, the antenna array delivers a main beam (with gain about 8.0 dBi) to the forward direction (z axis), as shown in Figure 4.9 to Figure 4.14; when the phase difference is 180^0 , the two elements radiations cancel each other along z direction hence result in a forward null as show in Figure 4.15 to Figure 4.17. Compared to Figures 4.9 to Figure 4.14 and Figure 4.15 to Figure 4.17, the phases in Figure 4.18 to Figure 4.20 and Figure 4.21 to Figure 4.22 have extra 80^0 phase. According to antenna array theory [7], this extra phase would tilt the radiation patterns by about 25^0. As expected, a tilted beam pattern and a tilted null pattern are exhibited in Figures Figure 4.18 to Figure 4.20 and Figure 4.21 to Figure 4.22, respectively.

CHAPTER 5

CONCLUSIONS

A wideband cavity backed slot antenna array is designed in this thesis report. This antenna is designed to be operated in an automobile-borne radar system. The use of a slot antenna instead of a patch antenna reduces the design complexities while maintaining a very wide impedance bandwidth. The use of inverted feed design improves the radiation performance of the antenna meaning that a higher pattern gain can be achieved. The use of a discrete cavity makes the slot radiation unidirectional. The discrete cavity also enables our antenna design to be fully planar as it is completely compatible with printed circuit fabrication process. When applied in an antenna array, it minimizes mutual coupling among the array elements. The layered design adopted along with the above mentioned features makes our inverted cavity backed slot antenna array easy to fabricate as we have shown by using a very basic fabrication process. The fabrication process used here, invariable has a couple of minor defects despite which our antenna yields excellent results thus making it mechanically robust.

Simulation carried out using Ansoft HFSS EM simulation software and measurement results (input impedance and radiation pattern) have excellent agreement. The measured input impedance bandwidth is 27.5%. By adjusting the feed phases monopulse beam-scanning is successfully demonstrated. It is therefore concluded that, this antenna array can be readily applied to ultra-wideband automotive radars.

In this thesis, antenna prototypes are simulated and measured around 3 GHz range as it is easier to control fabrication and measurement accuracies. Future re-

search includes scaling this antenna design to [22 GHz, 29 GHz] range, which is allocated for automobile-borne radars.

REFERENCES

[1] Automotive radars: From car collision avoidance to autonomous driving. In *Microwave Symposium Digest, 2002 IEEE MTT-S International*, 2002.

[2] Ultra-wideband communications and radar: Entering the marketplace. *IEEE MTT-S Int. Microwave Symp. Joint IMS/RFIC Focus Session, Philadelphia, PA*, 2003.

[3] FCC Washington DC ET Docket 98-153. First report and order, revision of part 15 of the commissions rules regarding ultra wideband transmission systems. 2002.

[4] P. Abele, A. Trasser, E. Sonmez, K.B. Schad, A. Munding, and H. Schumacher. A compact low-cost doppler sensor MMIC in SiGe technology for the ISM band at 24 GHz. In *Microwave Conference, 2004. 34th European*, volume 2, 2004.

[5] GR Aiello, GD Rogerson, D.T. Commun, and CA San Diego. Ultra-wideband wireless systems. *IEEE microwave magazine*, 4(2):36–47, 2003.

[6] HG Akhavan and D. Mirshekar-Syahkal. Approximate model for microstrip fed slot antennas. *Electronics Letters*, 30(23):1902–1903, 1994.

[7] C.A. Balanis. *Antenna theory*.

[8] CR Cockrell. The input admittance of the rectangular cavity-backed slot radiator. *IEEE Trans. Antennas Propagat*, 24:288–294, 1976.

[9] Germany High-tech Rep Daimler-Chrysler AG, Stuttgart. Cars with sense and sensibility, 2002.

[10] AD Droitcour, O. Boric-Lubecke, VM Lubecke, J. Lin, and GTA Kovacs. Range correlation and I/Q performance benefits in single-chip silicon Doppler radars

for noncontact cardiopulmonary monitoring. *IEEE Transactions on Microwave Theory and Techniques*, 52(3):838–848, 2004.

[11] GF Engen and CA Hoer. Thru-reflect-line: An improved technique for calibrating the dual six-port automatic network analyzer. *IEEE Transactions on Microwave Theory and Techniques*, 27(12):987–993, 1979.

[12] J. Galejs. Admittance of a rectangular slot which is backed by a rectangular cavity. *IEEE Transactions on Antennas and Propagation*, 11(2):119–126, 1963.

[13] F. Gallée, G. Landrac, and MM Ney. Artificial lens for third-generation automotive radar antenna at millimetre-wave frequencies. *IEE Proceedings-Microwaves, Antennas and Propagation*, 150(6):470–476, 2003.

[14] E.F. Greneker III. Radar sensing of heartbeat and respiration at a distance with security applications. In *Proceedings of SPIE*, volume 3066, page 22, 1997.

[15] I. Gresham, A. Jenkins, R. Egri, C. Eswarappa, N. Kinayman, N. Jain, R. Anderson, F. Kolak, R. Wohlert, SP Bawell, et al. Ultra-wideband radar sensors for short-range vehicular applications. *IEEE transactions on microwave theory and techniques*, 52(9 Part 1):2105–2122, 2004.

[16] M. Hajian, DP Tran, and LP Ligthart. Design of a wideband miniature dielectric-filled waveguide antenna for collision-avoidance radar. *IEEE Antennas and Propagation Magazine*, 42(1):34–40, 2000.

[17] K. Hamaguchi, H. Ogawa, T. Kobayashi, and R. Kohno. Development of Ultra-Wideband Short-Range Impulse Radar System for Vehicular Applications. *IEICE Transactions on Electronics*, 88(10):1922–1931, 2005.

[18] J. Hirokawa, H. Arai, and N. Goto. Cavity-backed wide slot antenna. In *IEE Proceedings H Microwaves, Antennas and Propagation*, volume 136, pages 29–33, 1989.

[19] C.Y. Kim, J.G. Kim, D. Baek, and S. Hong. A Circularly Polarized Balanced Radar Front-End With a Single Antenna for 24-GHz Radar Applications. *IEEE Transactions on Microwave Theory and Techniques*, 57(2):293–297, 2009.

[20] M. Klotz and H. Rohling. A 24 GHz short range radar network for automotive applications. In *Radar, 2001 CIE International Conference on, Proceedings*, pages 115–119, 2001.

[21] SI Latif, L. Shafai, and SK Sharma. Bandwidth enhancement and size reduction of microstrip slot antennas. *IEEE Transactions on Antennas and Propagation*, 53(3):994–1003, 2005.

[22] Q. Li and Z. Shen. An inverted microstrip-fed cavity-backed slot antenna for circular polarization. *IEEE Antennas and Wireless Propagation Letters*, 1, 2002.

[23] Q. Li and Z. Shen. Inverted microstrip-fed cavity-backed slot antennas. *IEEE antennas and wireless propagation letters*, 1, 2002.

[24] Q. Li, Z. Shen, and P.T. Teo. Microstrip-fed cavity-backed slot antennas. *Microwave and Optical Technology Letters*, 33(4):229–233, 2002.

[25] Y. Li, Q. Xue, E.K.N. Yung, and Y. Long. Two-dimensional beam-scanning microstrip leaky-wave antenna. *Electronics Letters*, 44:183, 2008.

[26] Y. Liu, Z. Shen, and CL Law. A compact dual-band cavity-backed slot antenna. *IEEE Antennas and Wireless Propagation Letters*, 5(1):4–6, 2006.

[27] K. Mandke, H. Nam, L. Yerramneni, C. Zuniga, and T. Rappaport. The evolution of ultra wide band radio for wireless personal area networks. *Spectrum*, 3:10–6, 2003.

[28] H.H. Meinel. Automotive Millimeterwave Radar History and present Status. In *European Microwave Conference, 1998. 28th*, volume 1, 1998.

[29] W. Menzel and D. Kessler. A Folded Reflectarray Antenna for 2D Scanning. *ITG-Fachbericht-GeMiC 2009*, 2009.

[30] A. F. Molisch and J. Zhang. Localization via ultra-wideband radios: a look at positioning aspects for future sensor networks. *Wireless Technology*, page 7881, 2003.

[31] T. Nakanishi, T. Yoshida, A. Ishida, H. Uno, and Y. Saito. Multiple-Loop Array Antenna with Switched Beam for Short-Range Radars. In *2006 IEEE 64th Vehicular Technology Conference, 2006. VTC-2006 Fall*, pages 1–5, 2006.

[32] Y. Pinto, C. Person, D. Gloria, A. Cathelin, D. Belot, S. Pruvost, and R. Plana. SIP antenna on 0.13 μm SiGe technology at 79 GHz for SRR automotive radar. *International Journal of Microwave and Wireless Technologies*, 1(06):529–536, 2010.

[33] D. Pozar. A reciprocity method of analysis for printed slot and slot-coupled microstrip antennas. *IEEE Transactions on Antennas and Propagation*, 34(12):1439–1446, 1986.

[34] D. Shively. Ultra-WIDEBAND RadioThe New Part 15. *HAND*, 60:70–80.

[35] A.H.F.S. Simulator. Version 10.0. *Ansoft Corporation*, 2005.

[36] Y. Tajima and Y. Yamada. Design of shaped dielectric lens antenna for wide angle beam steering. *Electronics and Communications in Japan (Part III: Fundamental Electronic Science)*, 89(2):1–12, 2005.

[37] X.J. Tang, S. Xiao, B.Z. Wang, and J. Wang. A 60-GHz wideband slot antenna based on substrate integrated waveguide cavity. *International Journal of Infrared and Millimeter Waves*, 28(4):275–281, 2007.

[38] T. Teshirogi, T. Kawamura, and A. Yamamoto. Wideband, high-gain printed antenna for uwb automotive radar. In *2007 IEEE Antennas and Propagation Society International Symposium*, pages 3868–3871, 2007.

[39] L. Xue and VF Fusco. 24 GHz automotive radar planar Luneburg lens. *Microwaves, Antennas & Propagation, IET*, 1(3):624–628, 2007.

[40] Y. Yoshimura. A Microstripline Slot Antenna (Short Papers). *IEEE Transactions on Microwave Theory and Techniques*, 20(11):760–762, 1972.

[41] M. Zechnall. The sensitive car. *Australian Electronics Engineering*, 34(9), 2001.

[42] B. Zheng and Z. Shen. Effect of a finite ground plane on microstrip-fed cavity-backed slot antennas. *IEEE Transactions on Antennas and Propagation*, 53(2):862–865, 2005.

BIOGRAPHICAL STATEMENT

Vinay Magadi Vikram is a researcher at Wave Scattering Research Centre. His research interests lies in different aspects of Radio Frequency (RF) and microwave design including RF & microwave circuits, ultra wide band (UWB) antenna design and RF & microwave calibration techniques. He is also interested in wireless communication, wireless networks and has good knowledge in Embedded design. He has authored 1 journal paper published in Electronic Letters.

Vinay received his Masters of Science degree in Electrical Engineering from University of Texas at Arlington, Texas and his Bachelor's in Electronics & Communication Engineering Visvesvaraya Technological University, India.